AGU ADVANCING EARTH AND SPACE SCIENCES

JGR Atmospheres

Key Points:

- Non-fossil sources have dominated (ca. 60%–70%) elemental carbon (EC) deposition in a Svalbard ice core between 1700 and 2005
- The contribution of fossil fuels to EC was highest between 1860 and 1920 and toward the end of the record starting in the 1960s or 1970s
- Atmospheric transport modeling indicates that observed increased EC deposition was associated with potential Asian sources in 1948–2004

Supporting Information:

Supporting Information may be found in the online version of this article.

Correspondence to:

M. M. Ruppel,
meri.ruppel@fmi.fi

Organic Compounds, Radiocarbon, Trace Elements and Atmospheric Transport Illuminating Sources of Elemental Carbon in a 300-Year Svalbard Ice Core

M. M. Ruppel[1,2] ⓘ, M. Khedr[3,4] ⓘ, X. Liu[3,4] ⓘ, E. Beaudon[5] ⓘ, S. Szidat[6,7] ⓘ, P. Tunved[8], J. Ström[8], H. Koponen[9], O. Sippula[9,10], E. Isaksson[11], J.-C. Gallet[11] ⓘ, M. Hermanson[12] ⓘ, S. Manninen[2], and J. Schnelle-Kreis[4] ⓘ

[1]Atmospheric Composition Unit, Finnish Meteorological Institute, Helsinki, Finland, [2]Faculty of Biological and Environmental Sciences, Ecosystems and Environment Research Programme, University of Helsinki, Helsinki, Finland, [3]Joint Mass Spectrometry Center, University of Rostock, Rostock, Germany, [4]Joint Mass Spectrometry Center, Cooperation Group Comprehensive Molecular Analytics, Helmholtz Zentrum München, German Research Center for Environmental Health, Neuherberg, Germany, [5]Byrd Polar and Climate Research Center, The Ohio State University, Columbus, OH, USA, [6]Department of Chemistry, Biochemistry and Pharmaceutical Sciences, University of Bern, Bern, Switzerland, [7]Oeschger Centre for Climate Change Research, University of Bern, Bern, Switzerland, [8]Department of Environmental Science, Stockholm University, Stockholm, Sweden, [9]Department of Environmental and Biological Sciences, University of Eastern Finland, Kuopio, Finland, [10]Department of Chemistry, University of Eastern Finland, Joensuu, Finland, [11]Norwegian Polar Institute, Tromsø, Norway, [12]Hermanson & Associates (LLC), Haarlem, The Netherlands

Abstract Black carbon (BC) particles produced by incomplete combustion of biomass and fossil fuels warm the atmosphere and decrease the reflectivity of snow and ice, hastening their melt. Although the significance of BC in Arctic climate change is widely acknowledged, observations on its deposition and sources are few. We present BC source types in a 300-year (1700–2005) Svalbard ice core by analysis of particle-bound organic compounds, radiocarbon, and trace elements. According to the radiocarbon results, 58% of the deposited elemental carbon (EC, thermal-optical proxy of BC) is of non-fossil origin throughout the record, while the organic compounds suggest a higher percentage (68%). The contribution of fossil fuels to EC is suggested to have been elevated between 1860 and 1920, particularly based on the organics and trace element data. A second increase in fossil fuel sources seems to have occurred near the end of the record: according to radiocarbon measurements between 1960 and 1990, while the organics and trace element data suggest that the contribution of fossil fuels has increased since the 1970s to the end of the record, along with observed increasing EC deposition. Modeled atmospheric transport between 1948 and 2004 shows that increasing EC deposition observed at the glacier during that period can be associated with increased atmospheric transport from Far East Asia. Further observational BC source data are essential to help target climate change mitigation efforts. The combination of robust radiocarbon with organic compound analyses requiring low sample amounts seems a promising approach for comprehensive Arctic BC source apportionment.

Plain Language Summary Black carbon (BC) is a fine particulate emission component formed in natural and anthropogenic combustion of biomass and fossil fuels. BC effectively warms the atmosphere, and when it is deposited on snow and ice, it hastens their melt. BC strongly amplifies Arctic climate change but information on its deposition variations and sources are still very scarce. We studied sources of BC in a Svalbard (high-Arctic) ice core covering the years 1700–2005 by analysis of chemical compounds, radiocarbon and trace elements. We found that throughout the ice core, the contribution of biomass combustion to BC was higher (ca. 60%–70%) than that of fossil fuels. The contribution of fossil fuel sources to BC in the ice core was elevated in 1860–1920, and again at the end of the record starting in the 1960s–1970s. Atmospheric transport modeling shows that increasing BC deposition observed at the glacier since the 1970s was associated with airmasses arriving increasingly from Far East Asia. Further observations on Arctic BC sources are essential to inform decision makers on which BC emissions most affect Arctic climate change.

1. Introduction

Black carbon (BC) particles are produced by incomplete combustion of carbonaceous material and have global adverse climate effects due to their strong absorption of visible light. The climate effect of BC is amplified in

the Arctic, as BC deposition on snow and ice hastens their melt (e.g., Bond et al., 2013). BC emissions occur by two processes: (a) natural (forest, peatland, and grassland) fires, and (b) in anthropogenic activities (e.g., transportation, residential burning, energy production, industry). BC has an atmospheric lifetime of a few days to weeks during which it may be transported over thousands of kilometers before deposition (Ramanathan & Carmichael, 2008). Atmospheric transport models suggest that emissions from East and South Asia, and Russia contribute most to the Arctic BC burden (AMAP, 2015; Backman et al., 2021; Sand et al., 2016). Within-Arctic emissions are particularly detrimental as they cause a five times stronger warming compared to equal emissions at mid-latitudes, as Arctic emissions are more likely to be deposited in the area (Sand et al., 2013).

Atmospheric BC concentrations have been monitored in the Arctic since 1989 at an increasing number of measurement stations (e.g., AMAP, 2015; Sharma et al., 2013), and several studies on modeled atmospheric BC concentrations in the Arctic exist (e.g., Eckhardt et al., 2015; Koch et al., 2011; Srivastava & Ravichandran, 2021). Pioneering studies on BC in Arctic precipitation (Mori et al., 2020; Sinha et al., 2018), and wide-ranging campaigns on BC concentrations in Arctic snowpacks have been conducted (e.g., Clarke & Noone, 1985; Doherty et al., 2010; Evangeliou et al., 2018; Forsström et al., 2013; Zdanowicz et al., 2021). Insights to past Arctic BC deposition beyond the era of atmospheric and snow monitoring data have been gained from ice core and lake sediment records (e.g., Ruppel et al., 2014, 2015, 2017, 2021; Eckhardt et al., 2023; McConnell, 2010; Osmont et al., 2018; Zdanowicz et al., 2021).

Currently, there is a critical lack of field measurements of Arctic BC sources hindering targeted emission cuts required for effective climate change mitigation (e.g., AMAP, 2015). Comprehensive observational data able to classify BC source types for the Arctic are available for atmospheric samples (Moschos et al., 2022a; von Schneidemesser et al., 2009; Winiger et al., 2017, 2019), and a limited amount of snow samples (Hegg et al., 2010; Macdonald et al., 2018; Rodriguez et al., 2020), and ice cores (e.g., McConnell et al., 2007; Osmont et al., 2018; Vega et al., 2015; Zennaro et al., 2014). Traditionally, source apportionment of Arctic BC has relied on proxies, that is, compounds released simultaneously with BC during combustion. For instance, ions such as non-sea-salt sulfate (SO_4^{2-}) and nitrate (NO_3^-) are well-known indicators of anthropogenic pollution detected from ice cores (e.g., McConnell et al., 2007; Vega et al., 2015). Ammonium (NH_4^+) has been used, among others (e.g., Jickells et al., 2003; Legrand et al., 2021; Liss & Galloway, 1993), as a proxy of biomass combustion-derived BC (e.g., Keegan et al., 2014; Sierra-Hernández et al., 2022).

In atmospheric science, source-specific organic markers have been long used to apportion the contributions of different sources to the particulate matter composition. Organic aerosol constituents have been used to describe natural and anthropogenic contributions to Arctic aerosols (Moschos et al., 2022a, 2022b; von Schneidemesser et al., 2009). Water soluble organic markers for biomass combustion such as vanillic acid, levoglucosan, or *p*-hydroxybenzoic acid have been recently introduced as biomass combustion proxies in Arctic ice cores (e.g., Grieman et al., 2018; Legrand et al., 2016; McConnell et al., 2007; Osmont et al., 2018; Zennaro et al., 2014). On the other hand, water-insoluble organic carbon (WIOC) or its components have rarely been studied in relation to the deposition of BC in Arctic snow or ice cores. More recently, state-of-the-art dual-carbon (radiocarbon ($\Delta^{14}C$) and stable carbon ($\delta^{13}C$)) isotope analyses on atmospheric (Winiger et al., 2017, 2019) and snow (Rodriguez et al., 2020) samples has allowed separation of BC sources first to biomass or fossil fuel combustion based on radiocarbon (Gustafsson et al., 2009), and further classification into coal, oil, or gas flaring with the stable carbon isotopic composition of BC particles (Andersson et al., 2015).

Several assessments call for additional field-based observations separating specific BC sources, as these are essential to evaluate and refine emission inventories used in climate modeling, and credible source apportionment is the underpinning of targeted climate change mitigation actions aimed at efficiently reducing BC emissions (e.g., AMAP, 2015; Bond et al., 2013). Here, we present unique and comprehensive elemental carbon (EC, a thermal-optical proxy for BC) source apportionment data from a Svalbard ice core covering 1700 to 2005 by non-polar organic hydrocarbons (n-alkanes and hopanes), supported by data of trace elements, analysis of EC radiocarbon data, and airmass transport analysis. Major ions and trace elements have long been used to study the influence of natural sources and anthropogenic activity in ice core records (e.g., Beaudon et al., 2017; Legrand et al., 2016; McConnell & Edwards, 2008; McConnell et al., 2007; Osmont et al., 2018). n-Alkanes and hopanes, on the other hand, have been widely used for the source apportionment of BC in atmospheric samples (e.g., Briggs & Long, 2016; Schnelle-Kreis et al., 2007; von Schneidemesser et al., 2009), while very few studies exist on their fluxes to mid-latitude ice cores (Miyake et al., 2006; Sankelo et al., 2013). To our knowledge, this is the first study to present n-alkane and hopane fluxes to an Arctic ice core, and to assess the use of these compounds in EC source apportionment in ice cores. Ice cores are
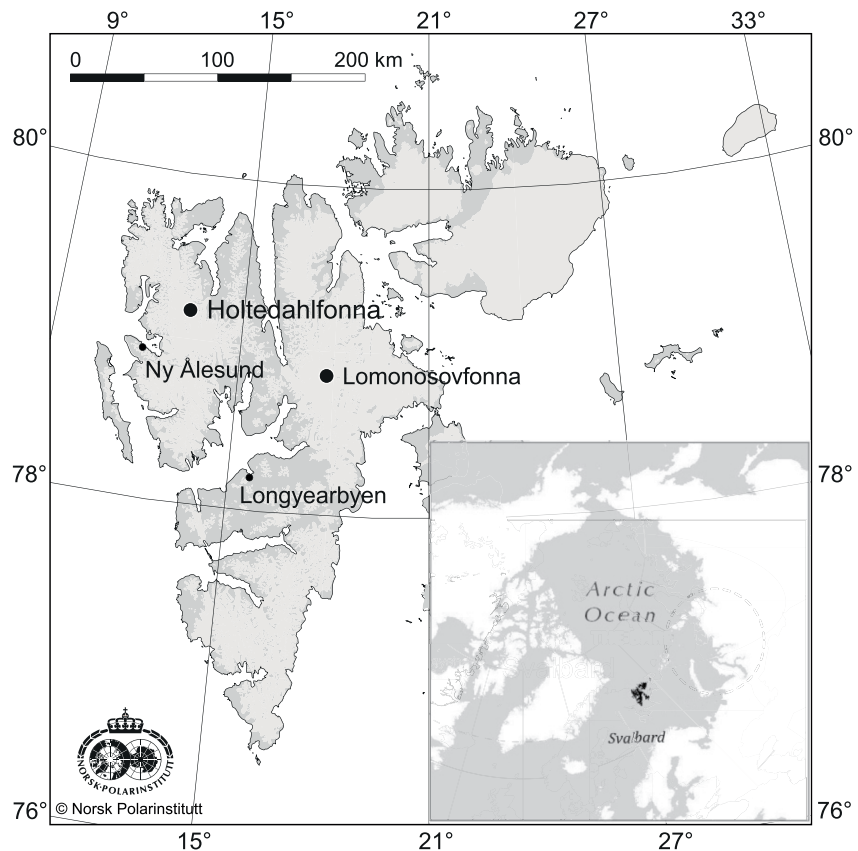
Figure 1. Map of Svalbard and location of the Holtedahlfonna glacier. Also shown are the Lomonosovfonna glacier from which another BC record exists (Osmont et al., 2018) and the settlements of Longyearbyen and Ny-Ålesund.

invaluable to understand BC deposition trends and sources beyond the observational period covered by atmospheric and snow samples. The acquired information helps to assess different BC emission sources affecting BC deposition in the Arctic and informs policy makers on how to mitigate Arctic climate warming.

2. Materials and Methods

2.1. Study Site, Previous Ice Core Sampling, Elemental Carbon Quantification

Svalbard is a Norwegian archipelago located in the Arctic Ocean (Figure 1) at the southern edge of permanent sea ice. Despite its location in the high Arctic, Svalbard has a relatively mild climate due to the North Atlantic Current and being on the pathway of Arctic and North Atlantic cyclones. About 60% of Svalbard is covered by glaciers, which have lost mass since the 1960s (Schuler et al., 2020). The mass loss has increased since 2000 (Schuler et al., 2020), and many Svalbard glaciers experience frequent summer surface melt (e.g., Beaudon et al., 2013). Holtedahlfonna glacier covers ca. 300 km^2, and is situated on northwestern Svalbard 40 km northeast of the Ny-Ålesund research station (Figure 1).

A 125 m deep ice core was collected from a saddle point of the Holtedahlfonna glacier (79°08′15′ N, 13°16′20′ E; 1150 m a.s.l.) in April 2005. Further details on the ice core extraction and sample handling are given in Beaudon et al. (2013) and for elemental carbon in Ruppel et al. (2014). In brief, after retrieval and frozen transportation to the Norwegian Polar Institute (Tromsø, Norway), parallel-sided sections from the inner part of the core were cut with a thin-blade band saw in a cold room (−22°C) and distributed for major ion (Beaudon et al., 2013) and elemental carbon (Ruppel et al., 2014) measurements (in addition to tritium (Van der Wel et al., 2011) and oxygen isotope (Divine et al., 2011) analyses that were used for the dating of the core, and organic contaminant analyses (Ruggirello et al., 2010)).

Ice samples cut in high resolution were pooled together (to ensure adequate carbon contents) for elemental carbon (EC, a thermal-optical proxy for BC) analyses, resulting in 88 samples that were melted and filtered through

pre-combusted (at 800°C for 4 hr) quartz fiber filters (Munktel). The filters were dried and placed into plastic holders that were wrapped in aluminum foil and stored in a refrigerator. A 1.5 cm^2 subsample of each filter was analyzed for EC using a thermal–optical method (TO, Sunset Laboratory Inc., Forest Grove, USA; Birch & Cary, 1996) with the EUSAAR_2 protocol (Cavalli et al., 2010) at Stockholm University (Ruppel et al., 2014). A maximum of 35%–40% total uncertainty is estimated to be related to these EC measurements caused by potential heterogenous particle loading on the filters (∼20% uncertainty) and smallest particles percolating through the filter (i.e., undercatch, ca. ∼22%) (discussed in more detail in Ruppel et al. (2014)).

2.2. Water Insoluble Organic Compounds Analyses and Source Apportionment

2.2.1. n-Alkane and Hopane Quantification

Water insoluble carbon (WIOC) composition from 50 selected filter samples were analyzed for n-alkanes and hopanes by thermal desorption gas chromatography time of flight mass spectrometry (TD-GC-TOFMS, Orasche et al., 2011) at Helmholtz Zentrum München. The analysis was implemented on a GC-Bench Top-TOFMS system (Leco, USA), equipped with a PAL-LINEX auto-sampler and a liner exchange system (Axel Semrau, Germany). The analysis included four internal standards and targeted 25 n-alkanes (carbon chain lengths of C_{16}–C_{40}) and 10 hopanes (Table S1 in Supporting Information S1). For analysis a 7 mm diameter circular aliquot was punched from the selected original EC filter samples, and spiked with 1 μL of the deuterated internal standards, and 1 μL of N-Methyl-N-(tri-methylsilyl)trifluoracetamid (MSTFA). Subsequently, the aliquots were placed in a GC liner, capped and incubated at 80°C for 1 hr to allow the MSTFA to deactivate active sites on the quartz fiber filter, which in turn increased analysis sensitivity. Then, the PAL-LINEX auto sampler de-capped the liner and placed it in the GC injector, where it was thermally desorbed at 300°C for 15 min, followed by a 59-min GC cycle. The data were acquired by the software ChromaTOF (Leco, USA) where peak assignment and integration was conducted manually, based on mass spectra matching and elution time, since the heavy background and frequent coelution in the samples hindered the commonly used consistent automatic peak identification and integration by the deconvolution algorithms in ChromaTOF. External calibration was done using authentic standards for the individual n-alkanes and 17α(H)21β(H)-30-Norhopan (29ab) for the hopanes. Duplicate measurements of 10 samples showed relative standard deviations of 25%–45% for the individual compounds. These duplicate measurements included both uncertainties related to the uneven particle loading on the filters and analytical uncertainties. n-Alkanes with chain lengths $<C_{21}$ were excluded from further analyses, as blank values for most samples exeeded sample values. All other values were blank corrected.

2.2.2. Using n-Alkanes and Hopanes to Apportion Source Contributions to EC Fluxes

Receptor models, such as positive matrix factorization (PMF), are mathematical tools for apportioning the contribution of sources to samples based on the composition or fingerprints of the sources (Paatero & Tapper, 1994). PMF has been used in numerous studies of source apportionment of particulate matter in ambient air (e.g., Galvão et al., 2021; Reff et al., 2007) where the goal is to identify and quantify the contributions of sources that contribute to particulate matter. The PMF accounts for the variable uncertainties often associated with environmental samples and enforces that all values in the solution profiles and contributions are non-negative, which is considered more realistic than the solutions of other methods such as principal component analysis. Thus, the goal of PMF is to solve the mass balance between measured species concentrations and source profiles, as shown in Equation 1, with the number of factors p, the species profile f of each source, and the amount g contributed by each factor to each individual sample.

$$x_{ij} = \sum_{k=1}^{p} g_{ik} f_{ik} + e_{ij} \tag{1}$$

where X is a data matrix of i by j dimensions, in which i number of samples and j chemical species measured, with uncertainties u_{ij} (Equation 2). p is the number of factors, f the species profile of each source, and g the amount contributed by each factor to each individual sample. e_{ij} is the residual for each sample/species.

The PMF then derives the factor contributions and profiles by minimizing the objective function Q:

$$Q = \sum_{i=1}^{n} \sum_{j=1}^{m} \left[\frac{x_{ij} - \sum_{k=1}^{p} g_{ik} f_{ik}}{u_{ij}} \right] \tag{2}$$

For the PMF analysis, we considered the quantitative data of the components for which measured values >limit of quantification (LOQ) were available in more than 60% of all samples. The deposition rates of EC, n-alkanes from docosane to hexacontane as well as the hopanes 29ab, 29ba, 30ab, 30ba, 31ab S and 31ab R were used. The relative standard deviations of the determined concentrations of individual compounds were used for the estimation of the uncertainty of the respective measured value. Measured values < LOQ were replaced with 1/2 of the respective LOQ. For these values, the uncertainty was set to 5/6 of the LOQ. Analyses were carried out using EPA PMF 5.0 Software (United States Environmental Protection Agency, 2014). Differing from the default settings of EPA-PMF 5.0, no negative values for source contributions were allowed in the analyses. For the analysis species with S/N ≤ 2.6 were set to weak.

PMF analyses based on WIOC mentioned above were performed to identify and allocate the major sources of the EC found in the ice-core samples. Analyses were performed for 2 to 4 factors, with the 3-factor solution giving the clearest interpretable result.

In addition to the WIOC based analyses, PMF analyses were performed including depositional flux results of water soluble of K^+ and NH_4^+ analyzed in Beaudon et al. (2013). Elevated concentrations of ammonium and potassium occur in smoke plumes from biomass burning (BB) compared to background concentrations (Andreae & Merlet, 2001). It was therefore proposed to use these as markers for BB. On the other hand, K^+ and NH_4^+ in Holtedahlfonna have a marine origin as well (Beaudon et al., 2013). As the estimation of non-sea-salt K^+ is difficult, we investigated the extent to which the inclusion of total water-soluble K^+ and NH_4^+ in the PMF analysis modifies the result for distinguishing fossil and non-fossil combustion sources of the EC.

2.3. Elemental Analyses

2.3.1. Analytical Method

Thirty one EC filter samples were selected for the analysis of 24 major and trace elements (TE) (Li, Be, Na, Al, Mg, K, V, Cr, Mn, Fe, Co, Ni, Cu, Zn, As, Rb, Sr, Ag, Cd, Sb, Cs, Ba, Tl, and Pb) by inductively coupled plasma mass spectrometry (ICP-MS, NeXION 350D, Perkin Elmer, USA). Prior to analysis, 1.5 cm^2 aliquots of the filter samples were digested, using first, a mixture (7:2) of nitric acid (65%–68%, Trace Metal grade, Fisher Chemicals) and hydrofluoric acid (40%, Trace Metal grade, Fisher Chemicals), and then, boric acid (4%, Suprapur grade, Merck). Then the digested samples were diluted with de-ionized water and transferred to the ICP instrument. The ICP instrument operation is described in detail in Lane et al. (2020). Scandium-45 was used as an internal standard, and a multi element standard (TraceCERT Periodic Table mixture 1, Sigma Aldrich) was used as a calibration standard. Filter blanks ($n = 6$) and standard reference material (NIST 1649a, urban dust) were digested and analyzed alongside the filter samples. Average blank values were subtracted from the TE analysis values. Note, that the NIST-1649a standard reference material does not contain Ag, Ba, Be, Cs, Cr, Li, and Tl.

The recovery of TEs in the standard reference material was on average 130%. The standard reference material was analyzed to estimate uncertainties in the methodology, not for correcting results. Based on the ca. 30% uncertainty in TE recovery of the reference material, and heterogenous particle loading on the filters (ca. 20% uncertainty (Ruppel et al., 2014)), we could estimate a total uncertainty of about 36% related to the TE analyses. Duplicate measurements of four samples ($n = 8$) showed the relative standard deviation of the TE measurements to vary between 1.6% (for Pb) and 100% (Li, Cr, As, Ba) with an average relative standard deviation of all TEs being 52%. These duplicate measurements included both uncertainties related to the uneven particle loading on the filters and methodological uncertainties in quantification, but the number of duplicate measurements were few. Altogether, this indicates a total uncertainty of 40%–50% for these measurements.

2.3.2. Crustal Enrichment Factor (EFc) Calculation

To investigate the potential of the TEs to signal anthropogenic versus natural emission sources we calculated their Crustal Enrichment Factor (EFc). The crustal enrichment factor is commonly adopted in environmental and ice core geochemical studies to characterize the non-crustal contribution (e.g., anthropogenic activities) of the element time series (e.g., Beaudon et al., 2017; Kaspari et al., 2009; Sierra-Hernandez et al., 2018). EFc is defined as: $\{[X]/[Fe]\}_{filter}/\{[X]/[Fe]\}_{UCC}$, where $\{[X]/[Fe]\}_{UCC}$ is Upper Continental Crust (UCC) reference (Wedepohl, 1995) used to normalize the filter sample mass ratio of the element of interest (X) to that of a conservative crustal element (here Fe). Typically, EFc deviations larger than 10 are interpreted as possible non-crustal influences.

2.4. Radiocarbon Analyses of EC

Fourteen original filter samples were selected for radiocarbon (^{14}C) analyses of EC. The amount of filter material left after all the previously described analyses was greatly restricted, and the samples for radiocarbon analyses were selected so that they (a) contained sufficient amount of carbon to allow the measurements, and (b) were as evenly as possible distributed over the ice core record (i.e., gaps in the data are caused by insufficient carbon and filter material available for radiocarbon measurements from those time periods). Carbonates were removed (Uglietti et al., 2016) and EC was then extracted from the filters and analyzed for radiocarbon as described in Y. L. Zhang et al. (2012), Szidat et al. (2014) and further refined in Rauber et al. (2022). In brief, ^{14}C of EC was measured using a Sunset OC/EC analyzer (Model 5L, Sunset Laboratory, USA) coupled with the accelerator mass spectrometer Mini Carbon Dating System (MICADAS) at the Laboratory for the Analysis of Radiocarbon (LARA; Szidat et al., 2014). Prior to the ^{14}C measurement, the filters were treated 3 times for carbonate removal under a fume hood by adding 50 µL of 1M HCl followed by air drying (Uglietti et al., 2016, T. Singer, personal communication). A further water extraction of the filters for removal of the water-soluble organic carbon to minimize the positive artifact from OC charring (such as done in Rauber et al., 2022; Y. L. Zhang et al., 2012) was not necessary, as this step was already included during filtration of the melted ice samples (see Section 2.1). The extracted filters were thermally desorbed in the OC/EC analyzer during the first three steps of the Swiss_4S protocol, volatilizing the remaining water-insoluble organic carbon from the filter (Y. L. Zhang et al., 2012). Thereby, EC was isolated onto the filters with average EC yields of 79 ± 7% and charring formation of pyrolyzed OC of 12% ± 7%. EC was quantified during the EC steps of the Swiss_4S protocol and the volatilized CO_2 was directed to the MICADAS system for ^{14}C analyses. $F^{14}C(EC)$ was extrapolated to 100% EC yield and corrected for pyrolyzed OC with a thermal-desorption model (Rauber et al., 2022; Rauber & Salazar, 2022).

The ^{14}C results are the modern fractions of the measured carbon ($F^{14}C$; Reimer et al., 2004), which is expressed as:

$$F^{14}C = \left(^{14}C/^{12}C\right)_{sample} / \left(^{14}C/^{12}C\right)_{1950} \tag{3}$$

where $\left(^{14}C/^{12}C\right)_{1950}$ is the reference isotopic ratio in 1950. The $F^{14}C$ values were corrected for the above-ground nuclear bomb tests in the 1950s and 1960s by dividing the reference value ($f_{nf,ref}$) that corresponds for the age of the individual sample to obtain the non-fossil fractions (f_{nf}) of carbon:

$$f_{nf} = F^{14}C / f_{nf,ref} \tag{4}$$

An average uncertainty of ca. 20% is related to the $F^{14}C$ results.

2.5. Atmospheric Transport Modeling

Airmass back trajectories (each running 10 days back in time) were calculated for every 4 hr interval between 1948 and 2004 to explore the major source areas for particles deposited at the Holtedahlfonna glacier and potential changes in the dominant transport patterns over the past decades. The model used was HYSPLIT version 5.0.0 (Stein et al., 2015), and the meteorological archives used was the NCEP/NCAR Global Reanalysis Data Archive (https://wesley.wwb.noaa.gov/reanalysis.html). The NCEP/NCAR archive is available from 1/1/1948 and has a resolution of 2.5° in the horizontal (90N–90S and 0E−357.5) and 16 levels in the vertical. Data is outputted every 6 hr. Besides provision of hourly endpoint values of latitude-longitude pairs and altitude along the trajectories, HYSPLIT has been run to provide also auxiliary meteorological information along the trajectories, and information for relative humidity, temperature, pressure, precipitation and topography was stored along with the other information.

The trajectories were organized according to the estimated time period covered by each ice core EC sample from 1948 to 2004. As each sample period represents multiple years the common approach of linking individual trajectories to hourly, daily or even seasonal averages is not feasible. Instead, characteristic properties were calculated for each ice core EC sample period. Most important of these is the footprint which is defined as the transport probability function, or $P_{i,j}$:

$$P_{i,j} = \frac{n_{i,j}}{N} \tag{5}$$

where $n_{i,j}$ is the number of trajectories that has resided over grid (i,j) for the sampled period and N is the total number of trajectories.

$P_{i,j}$ was on average based on roughly 4,000 trajectories per ice core sample, varying slightly with the estimated time period derived from the analysis of the ice cores. The analysis of the footprint, or rather the transport function $P_{i,j}$, was subsequently used to study source dependence on derived EC and ion content of the ice core samples. Statistical properties of trajectory altitude, relative humidity, and calculated precipitation were also calculated.

3. Results and Discussion

3.1. n-Alkanes and Hopanes

3.1.1. n-Alkane and Hopane Fluxes and Suggested Emission Source Classes

To our knowledge, these are the first n-alkane and hopane fluxes reported from an Arctic ice core. With the current filter-based methodology we were able to quantify only water insoluble particle-bound organic compounds. Unfortunately, specific organic biomass combustion markers could not be quantified here, as they are water-soluble, and thus were lost with the discarded filtrate.

After blank subtraction, temporal trends of 18 n-alkanes could be reasonably quantified. The n-alkane fluxes varied between <LOQ (about 0.02 μg m^{-2} yr^{-1} for n-alkanes) and 14.9 μg m^{-2} yr^{-1} (for tetracosane, Table S1 in Supporting Information S1). The results are presented in Figure 2 as standardized fluxes (calculated by subtracting the mean and dividing by the standard deviation), to visualize temporal trends of the compounds, as otherwise possibly higher concentrations of a specific compound compared to others would dominate the general trend. The n-alkanes were separated into three different groups (Figures 2b–2d) based on the length of their hydrocarbon chains, as these are known to coarsely relate to emissions from different emission sources (see below). Results on n-alkanes with the carbon chain lengths of 17–21 are not presented here as too few samples exceeded the LOQ and blank values. The hopane fluxes varied between <0.00002 and 1.47 μg m^{-2} yr^{-1} (for 17β(H)21α (H)-hopan (30ba) and 17α(H)21β(H)-hopan (30ab), respectively). The temporal variation in the hopane fluxes is presented in Figure 2e.

Generally, the n-alkane and hopane fluxes show similarities with several concurrently occurring peaks shown in Figure 2. The fluxes were low in the 1700s, increasing slightly in the early-1800s and clearly after 1850. Significant peak fluxes occurred for all n-alkanes and hopanes in the 1860s and 1880s, followed by generally slightly decreasing fluxes after that, and less dominant peaks in the early-1900s and for some n-alkanes and hopanes around 1950. After 1970 all n-alkanes and hopanes show rapidly increasing fluxes toward the end of the record, with the highest fluxes of the whole record reached during the last decades, particularly for many n-alkanes. The n-alkane and hopane fluxes show many similar features as the EC trend of the ice core (Figure 2a), including peak fluxes between 1850 and 1920, in 1950–1960 and again after 1970.

As specific n-alkanes and hopanes are released predominantly, but not exclusively, from different fuels, it is possible to get indications of their combustion sources by calculating ratios of their occurrence in samples. n-Alkanes can be divided into three partly overlapping emission source related classes depending on their chain length and carbon preference index (CPI, ratio of the concentrations of odd n-alkanes divided by the concentrations of even n-alkanes) (e.g., Yadav et al., 2013). Emissions from internal combustion engines (road, rail and marine) are sources of n-alkanes with different chain lengths. Vehicles emit n-alkanes with chain lengths in the range of C_{19}–C_{32} with C_{max} at C_{20} and C_{25} (gasoline vehicles) and at C_{20} for different diesel vehicles (Rogge et al., 1993; Schauer et al., 1999). While n-alkanes with a chain length around C_{20} mostly originate from unburned fuel (Brandenberger et al., 2005), n-alkanes with a chain length around C_{25} mainly originate from lubricating oil (Sakurai et al., 2003). Emissions from ships contain n-alkanes in the same range of chain lengths (Sippula et al., 2014). Biogenic sources (plant abrasion and biomass combustion) mostly show maximum n-alkane concentrations at chain lengths of C_{25}–C_{31} (Orasche et al., 2012; Oros & Simoneit, 1999), but coal combustion also may contribute to the n-alkanes with these chain lengths (Oros & Simoneit, 2000). A carbon preference index (CPI$_{25-33}$, calculated as $(0.5 * C_{25} + C_{27} + C_{29} + C_{31} + 0.5 * C_{33})/(C_{26} + C_{28} + C_{30} + C_{32})$) value of close to 1 (no preference) indicates a mature petroleum origin. While values slightly above 1 may well come from less mature fossil sources, for example, lignite (Oros & Simoneit, 2000), values greater than 3 clearly indicate biogenic origin.

The CPI is often used to estimate contributions of fossil and biogenic sources to n-alkanes. In the studied ice core, the CPI presented in Figure 3 averages about 1.5. Hence, in a range where a mix of contributions from both fossil (oil and coal) and biogenic sources can be assumed. Comparably high values (CPI > 2.5) were found in only few samples. Except for two cases (samples around ca. the years 1901 and 1996) high CPI do not coincide with high EC values and thus indication of biogenic combustion sources of EC seems quite weak in the ice core. On the
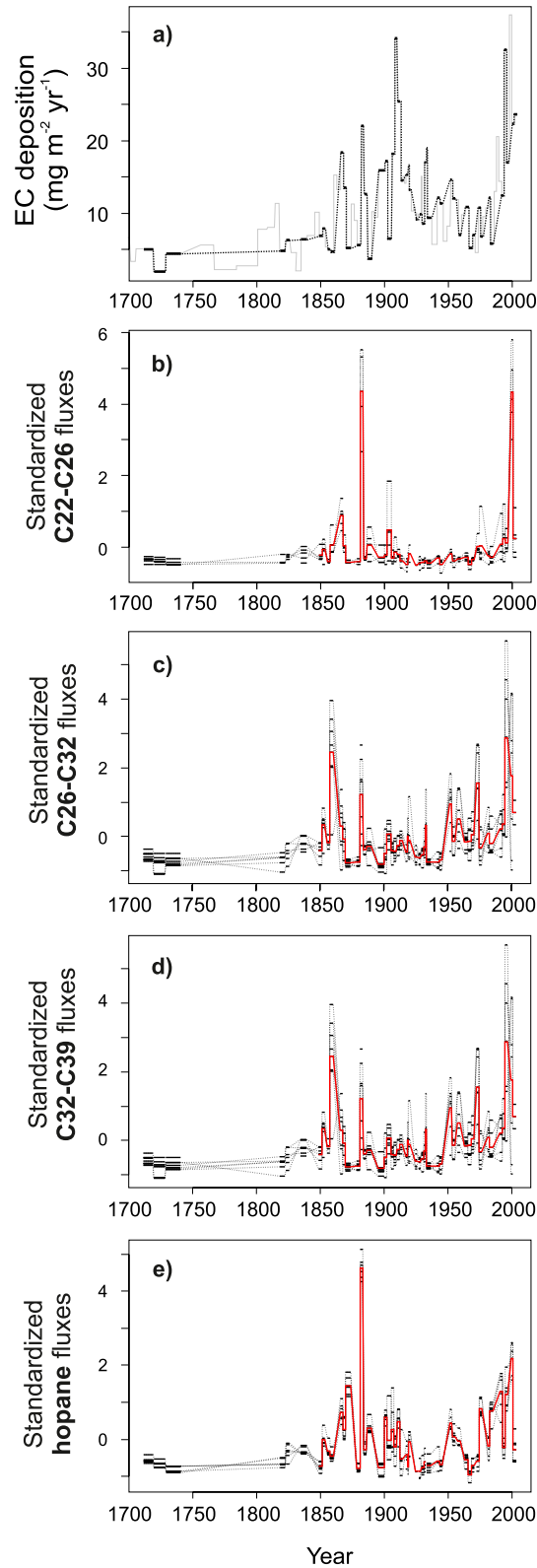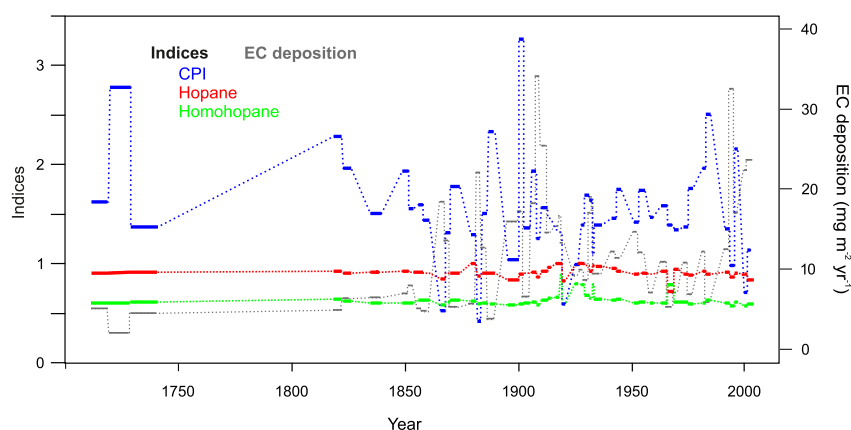
Figure 2.

Figure 3. Temporal trends of the CPI_{25-33} and hopane indices compared to the elemental carbon deposition trend. The dashed lines do not indicate analytical values but connect data points and are intended to follow the respective trend.

other hand, some of the samples with high EC contents show comparably low CPI values (e.g., around ca. 1866, 1882, 1994, and 2000–2004), that is, significant influences of petroleum-based sources.

The investigated hopanes are exclusively fossil fuel biomarkers. Due to their high stability, they have been found in emissions from the combustion of coal (Oros & Simoneit, 2000) or fuel oil (Rogge et al., 1997) but also from motor vehicles (Rogge et al., 1993) and ship engines (Sippula et al., 2014). In principle, hopane patterns differ significantly depending on the type and maturity of the fossil source. The hopane index (30ab/(30ab + 30ba)) is >0.9 in crude oil and 0.1−0.6 in different types of coal. In typical petroleum, the R/S-epimerization at C_{22} has an equilibrium S/(S + R) ratio, the so-called Homohopane index (i.e., 31abs/31abs + 31abR) is about 0.6 whereas this ratio ranges from about 0.1 for lignite coal to ∼0.4 for bituminous coal (Oros & Simoneit, 2000).

Hopane indices show relatively constant values over the entire period (Hopane index 0.91 ± 0.05 and Homohopane index 0.63 ± 0.06) (Figure 3). The comparatively small increase in the indices between 1915 and 1945 is probably due to increased uncertainty following very low observed hopane concentrations. The observed hopane patterns indicate a strong dominance of petroleum-based sources contra coal combustion for this substance group. This is unexpected, since according to emission inventories (e.g., Bond et al., 2007) there was no significant use of petroleum as a fuel before the mid-nineteenth century. We investigated coal samples collected in August 2022 from coal piles at the harbor of Longyearbyen, Svalbard (Figure 1), waiting to be exported, and found that, unlike coal mined in central Europe (Oros & Simoneit, 2000), the hopane pattern of coal mined in Svalbard (and mostly exported and used in Europe and Russia) very much resembles the hopane pattern found in mineral oils (hopane index > 0.9, homohopane index about 0.6). Thus, the use of Svalbard coal both locally and its import areas could potentially partly conceal the hopane pattern of other coal combustion-derived EC.

3.1.2. Source Apportionment of EC Based on n-Alkane and Hopane Fluxes

Three factors that contributed to the fluxes of deposited WIOC and EC were separated using PMF. Two of these factors are associated with significant amounts of EC while the third factor does not contribute to EC.

The first factor contributes 32% to the EC (Figure S2 in Supporting Information S1, top). It is characterized by high proportions of the hopanes (>80% to 100%) and only low proportions of n-alkanes. The maximum of n-alkane fluxes in this factor is at chain lengths of C_{27} to C_{29} with no preference for odd n-alkanes. Based on these characteristics, the factor is classified as fossil fuel (FF) combustion. The second factor contributes 68% to the EC (Figure S2 in Supporting Information S1, middle). It is characterized in particular by high contributions of n-alkanes in the C_{28}–C_{31} range and negligible proportions of hopanes (<5%). The CPI_{25-33} of this factor is 1.4. In summary, this factor is classified as non-fossil combustion (NF). The third factor does not contribute to the EC. It is characterized

Figure 2. EC deposition (mg m^{-2} yr^{-1}) (data from Ruppel et al. (2014)) compared to standardized (standard deviation units) n-alkane and hopane fluxes at Holtedahlfonna. The solid gray line in (a) presents the full EC record from the ice core while the black lines present the samples that were analyzed also for the organics. (b–d) The n-alkanes are separated into four groups based on their carbon chain lengths which may be representative of compounds produced by different processes. The red line in (b–e) presents the average of the respective compounds (black lines) in the sample groups. The dashed lines do not indicate analytical values but connect data points and are intended to follow the respective trend.
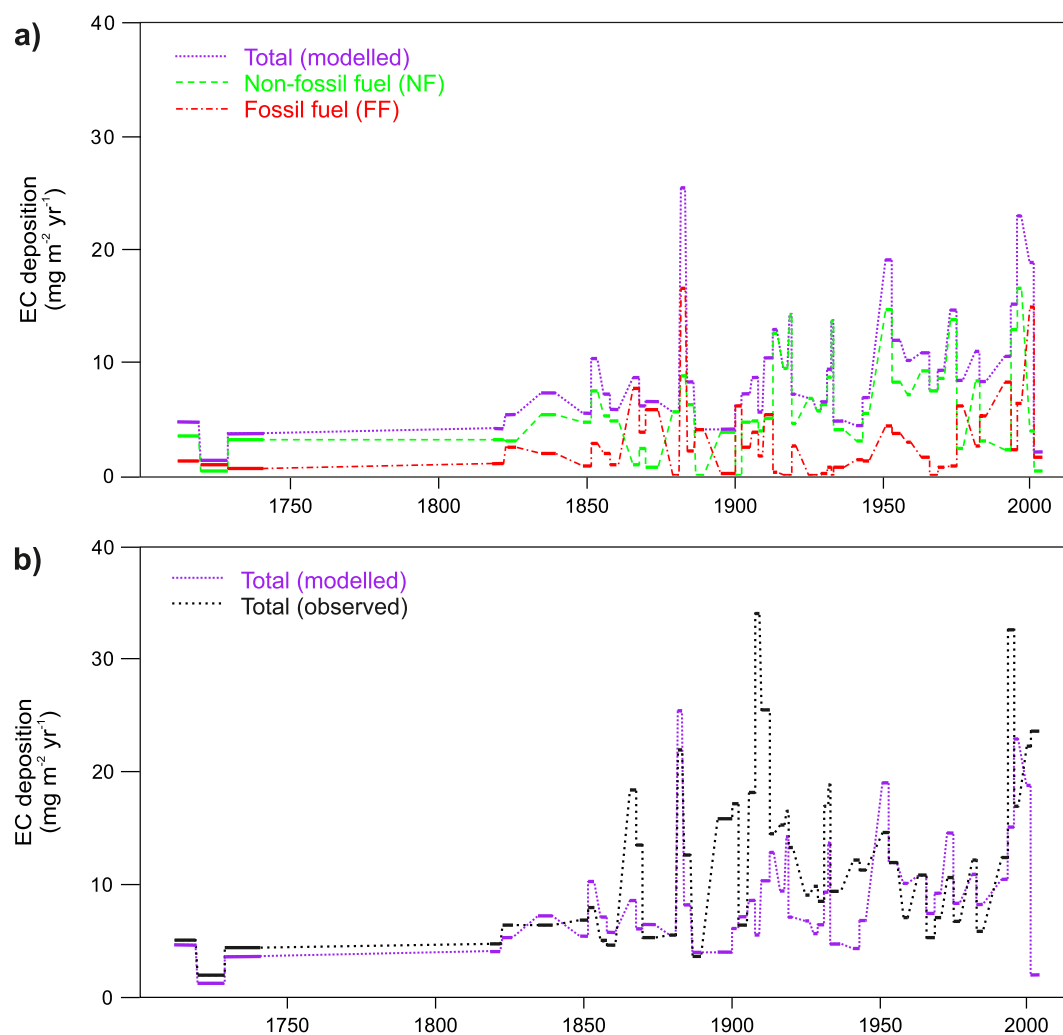
Figure 4. Contributions of fossil fuel (FF) and non-fossil fuel (NF) combustion to the modeled elemental carbon (EC) deposition in mg m^{-2} yr^{-1}. (a) Fossil fuel (red) and non-fossil fuel (green) sources of the modeled total EC deposition (mg m^{-2} yr^{-1}) based on the PMF analyses (purple) of organic compounds. (b) The modeled EC deposition (purple) compared to the observed EC deposition (black) for the organic compound samples (50 out of original total 88 filter samples). The analyzed samples are presented as thick lines for the time period covered by the respective sample. The dashed lines do not indicate analytical values but connect data points and are intended to follow the respective trend.

by relatively high proportions of n-alkanes $<C_{26}$ and medium to high proportions of n-alkanes $>C_{30}$. Since this factor does not contribute to the EC, it is not classified and will not be discussed below. Inclusion of water-soluble biomass-combustion associated K$^+$ and NH$_4^+$ ions available from the same ice core (Beaudon et al., 2013) in the PMF analyses (Figure S3 in Supporting Information S1) did not essentially change these results, which supports the factor classification achieved in the PMF analyses based on the organics (see Text S1 in Supporting Information S1).

The contributions of the FF and NF factors to the modeled EC deposition are shown in Figure 4a. The temporal variation of factor contributions to EC can be roughly divided into four periods. The period before 1860 is characterized by comparatively stable low EC values and on average high contributions of NF to EC. Between about 1860 and 1913, a few samples with high EC values were found. At the same time, the proportions of NF and FF fluctuate comparatively strongly during this phase. However, it must be noted that the high EC deposition fluxes observed in the ice core EC measurements in the period from 1895 to 1913 (and the last sample of the record) are poorly represented by the model, while generally the observed and modeled EC fluxes correlate significantly ($p < 0.005$) at $R^2 = 0.43$ (Figure 4b). The period from the beginning of World War I (1914) until the 1970s is characterized by medium EC fluxes and generally high shares of NF in the EC. Since the early 1970s, a gradual increase of FF for the EC fluxes can be stated. During this period, only two events with comparatively high proportions of NF for the EC were found.
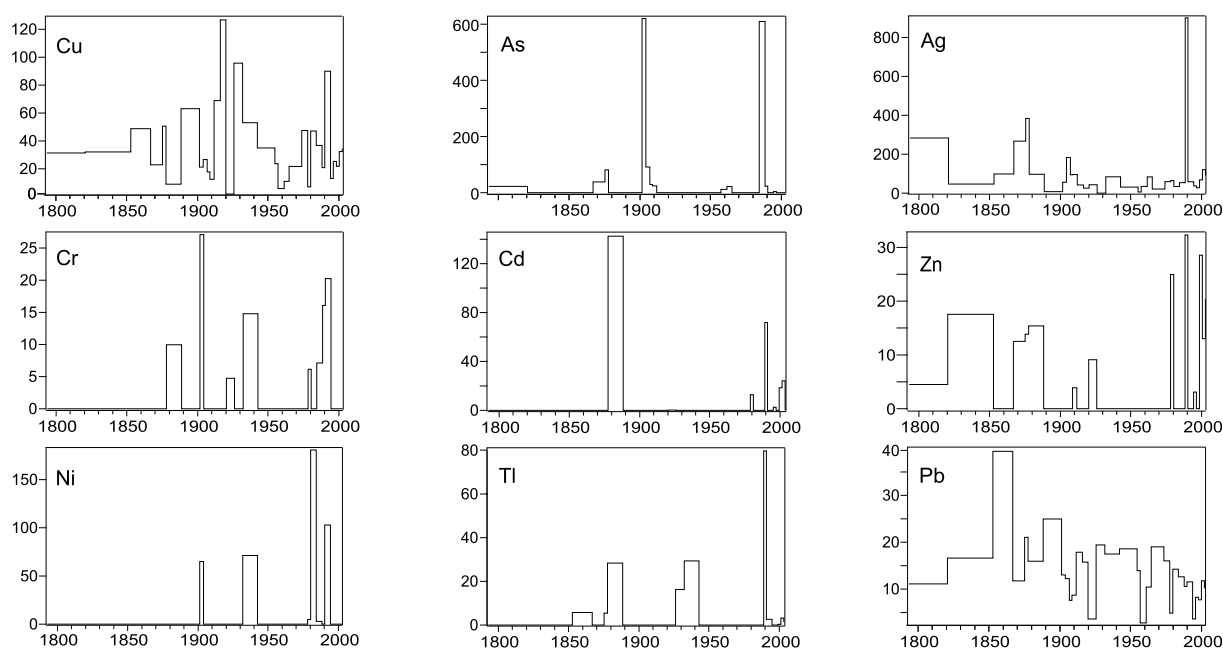
Figure 5. Crustal enrichment factor (EF) trends for trace elements that are enriched in the ice core relative to Fe (flux shown in Figure S1 in Supporting Information S1) and the upper continental crust reference. Values above 10 are considered significantly enriched.

Unexpectedly, the organic compound analyses, in particular the CPI and hopane indexes, did not point to a gradual shift from coal dominated combustion to increased oil use from 1850 to 1940, as other Arctic BC records (e.g., McConnell & Edwards, 2008) and emission inventories (e.g., Bond et al., 2007) suggest. The reason for this remains largely unresolved but a potential explanation is that the hopane pattern of coal produced in Svalbard and mainly exported to Europe and Russia for use resembles the hopane pattern of mineral oil which could partly mask the effect of other coal-combustion-derived particles on the recorded hopane pattern. The EC deposition at the high-altitude glacier is more affected by long-range transport than local sources (Aamaas et al., 2011; Forsström et al., 2013; Ruppel et al., 2014; Zdanowicz et al., 2021), and thus local use of Svalbard coal is not expected to significantly influence the hopane pattern of the ice core. Another possible, yet unlikely, explanation not investigated hitherto would be that the chemical processing of hopanes associated with the BC deposited with and on snow would lead to alterations of the chemical pattern.

3.2. EC Sources Suggested by Trace Element Fluxes

Details on the measured major and trace element concentrations and fluxes are given in Figure S1 and Table S2 in Supporting Information S1. Only a few of the 24 analyzed major and trace elements are enriched in the ice core, that is, have crustal Enrichment Factor (EFc) deviations of more than 10. Thus, most of the trace elements (TEs) in the ice core are of crustal origin. The temporal trends of the enriched TE fluxes are presented in Figure 5.

The enriched trace elements are Ag, As, Cd, Cr, Cu, Ni, Pb, Tl, and Zn. All of these have known origin from combustion of coal, oil or gas and in metallurgical activity (Pacyna & Pacyna, 2001; Tian et al., 2015). As for many of the other TEs, also for the enriched elements the concentrations were below the detection limit of the IPC-MS for most samples. Consequently, as there is no continuous time series available for the TEs, it is not reasonable to attempt any multivariate analysis to find correlations between them. Despite this, some general features are common for the fluxes of the enriched elements. Many of the TEs have peaks soon after the start of the industrialization, around 1860 and around 1880. Particularly, predominantly oil combustion-derived Tl and Cd, as well as Cr, show a peak around 1880, just like n-alkanes and hopanes (Figure 2). Notably, the TEs do not show a pronounced increase around 1910, while EC deposition shows a clear peak in this time. This early twentieth century EC peak is well known from Greenland ice cores and is attributed to coal combustion mainly in North America (e.g., McConnell & Edwards, 2008; McConnell et al., 2007). Rather, the mostly oil combustion-derived Ni, Tl and Cr show yet another simultaneous peak in the late 1930s, possibly associated with WWII. However, despite the discontinuity of the TE data, the enriched anthropogenic TEs seem to suggest comparably elevated

deposition post-1970 (Figure 5). A clear exception is Pb, of which emissions have been actively cut since the 1970s by the U.S. Clean Air Act and similar legislation in other countries due to known adverse health effects.

3.3. Fossil Fuel Versus Biomass Combustion Sources of EC Based on Radiocarbon and Organics Analyses

3.3.1. Comparison of Fossil Versus Non-Fossil Source Trends Determined by Radiocarbon and Organic Compounds in the Svalbard Ice Core

According to the radiocarbon analyses an overall average of 58% of the observed EC in the ice core is identified as of non-fossil origin. This fraction of biomass-derived EC is similar or higher than previously reported for atmospheric EC on Svalbard in 2009 and 2012–2013 (52% and 41%, respectively, Winiger et al., 2015, 2019). Simultaneous measurements of EC sources in precipitation versus atmospheric samples at the same site have also shown precipitation to contain higher contributions of biomass-derived EC than atmospheric samples (Rodriguez et al., 2020; Y. L. Zhang et al., 2015).

In the Holtedahlfonna ice core the fraction of biomass-derived EC varied between 38% and 70% over the studied period as shown in Figure 6. The radiocarbon results suggest that the contribution of biomass combustion to the total EC was ca. 50% or below before 1850, while EC deposition was very low at this point in absolute values (e.g., Figure 4b). Subsequently, the fraction of non-fossil EC peaked at 65%–68% in 1913–1961 after which it quickly declined to 43%–46% recorded in the mid-1960s to early 1990s. After the early 1990s the fraction of radiocarbon analyses-based non-fossil EC increased again to 70% in the early 2000s (Figures 6a and 6b).

The source attribution trend of fossil versus non-fossil fuels to the total EC statistically modeled from the organic compound data indicates some similar temporal variation as the EC sources based on the radiocarbon data (Figures 6a and 6b). For instance, the fraction of biomass combustion to EC remained large over the period of the two World Wars (ca. 1910 to 1950), as suggested both by the organic compound and radiocarbon data (Figures 6a and 6b). This matches also with the trend of European domestic combustion, which is dominantly based on biomass combustion and was by far the biggest emitter in this time period (e.g., Bond et al., 2007).

However, organic compound data seem more variable and some of the changes of fossil versus non-fossil fuel contributions to the EC seem temporally inconsistent with the radiocarbon data. First, according to the organics the contribution of fossil fuels to EC increased significantly only in ca. 1975 while this shift in sources is suggested by the radiocarbon analyses to have occurred already in the mid-1960s (Figure 6a). Second, the organics data suggest that after 1975 fossil fuel sources clearly dominated over non-fossil sources (e.g., Figure 6b) except for a biomass combustion peak around 1993 to 1997 (Figure 4a), while the radiocarbon data suggest that biomass combustion sources affected the ice core more strongly than fossil fuels since 1995 (Figures 6a and 6b). The mismatch seems to suggest that the source apportionment based on the organics might suffer from errors at the end of the ice core record. A weakness of the organic compounds together with the used PMF analyses is that the modeled EC deposition flux does not necessarily fit together with the observed EC deposition trend (Figure 4b). In our case, the model generally underestimates EC deposition, and particularly for many EC deposition peaks, such as ca. 1860s, 1890s, the highest peak in ca. 1910, and in the 2000s. Thus, the results on the potential sources of EC during these peaks based on the organic compound data are unfortunately not very reliable, although the general separation between fossil and non-fossil sources seems credible (see also Section 3.1.2 and Text S1 in Supporting Information S1).

3.3.2. Comparison of Fossil Versus Non-Fossil Source Trends in the Svalbard Ice Core With Northwestern Russian Lake Sediments

At the same time, the temporal variation of the contribution of non-fossil and fossil fuels to the total EC deposition based on radiocarbon analyses at Holtedahlfonna resembles greatly the one acquired from radiocarbon analyses of soot-BC extracted with a chemothermal oxidation method from lake sediments in the northwestern Russia flaring area (Figure 6c), an important source area for the Svalbard glacier, between 1800 and 2013 (Ruppel et al., 2014, 2021). In both records the contribution of non-fossil sources to EC peaked in the 1930s–1950s. After that fossil-fuel combustion seemed to dominate the records between 1960s and 1990s, but the fraction of non-fossil sources increased again to high values after early 1990s. As these radiocarbon analyses have been made from different environmental matrices (sediment and ice core) by different methodologies for BC extraction and thus partly different fractions of BC particles being analyzed, the general trend of biomass combustion-derived
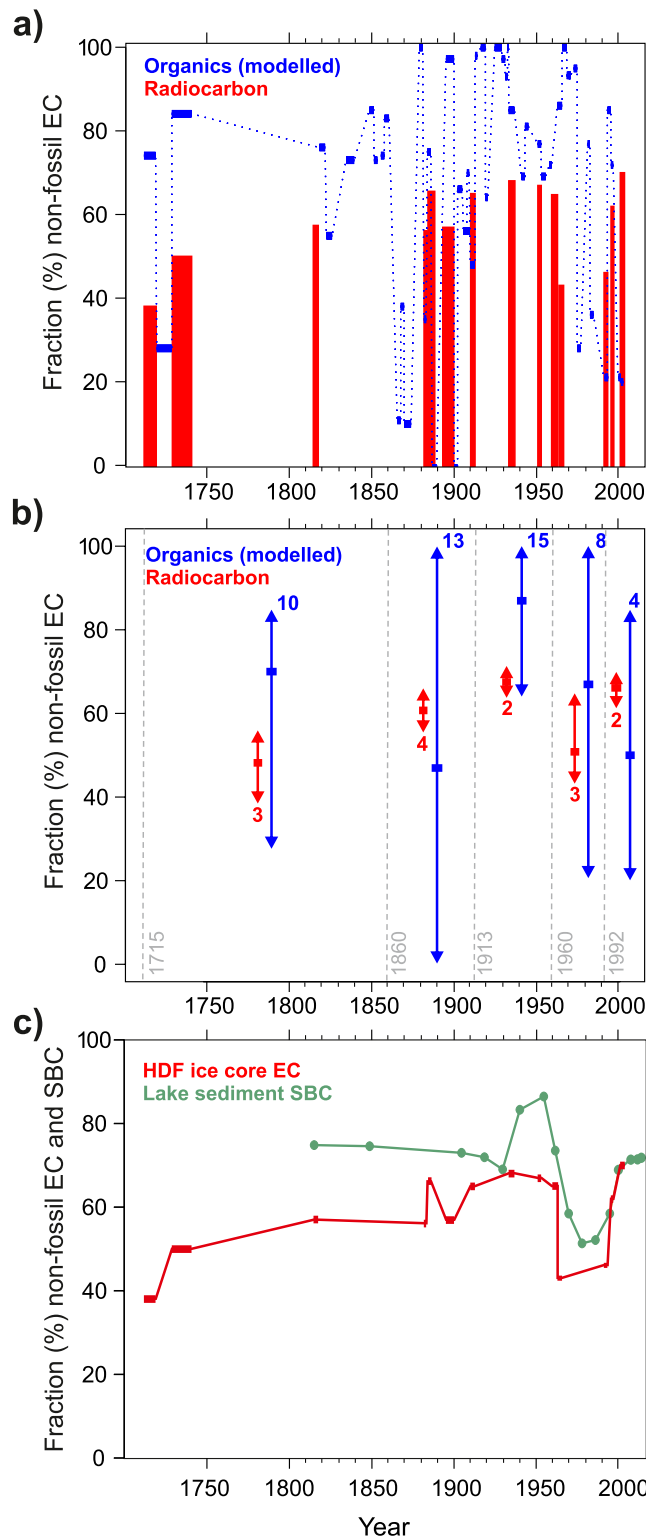
Figure 6.

BC deposition suggested by both these records seems strikingly robust. In Ruppel et al. (2021) the temporal trend in source composition was attributed to long-range (hundreds to thousands of km) transport of BC onto which regional (tens to hundreds of km) signals were superimposed, particularly strongly between ca. 1930 and 1990 by the coal and oil production history in north-western Russia (peaking between 1970 and 1990).

A surprising feature in the organic compound and radiocarbon records is the high contribution of fossil-fuel-derived EC in the 1700s and early 1800s before the onset of industrialization. The radiocarbon data suggests a contribution of 44%–62% and the organics data 16%–72% of fossil fuel-derived EC in this time period (Figures 6a and 6b). The absolute EC deposition was very low in this time period but still the percentage based on radiocarbon and organics analyses seems surprisingly large in a time period where fossil fuel combustion must have been marginal. Ruppel et al. (2021) found similar numbers in early 1800s for the contribution of fossil fuel combustion to SBC deposition in a north-western Russian lake sediment record (Figure 6c) and attributed this to peat combustion. The radiocarbon value of peat combustion-derived BC varies according to the age of the combusted peat. In northern Eurasia peats are on average ca. 5,000−6,000 years old (Mäkilä et al., 2013; Ruppel et al., 2013), and their combustion-derived BC would equal the radiocarbon signal of a 50% fossil fuel source, as the half-life of radiocarbon is ca. 5,700 years. In boreal environment peats have been used as an energy resource for over 2,000 years (World Energy Council, 2013). In the Arctic, very old peat layers can be reached close to the surface, such as ca. 6,600 years at 39 cm depth in northern Russia (H. Zhang et al., 2018), increasing the likelihood of these old peats being used as fuel. Furthermore, whaling was intense in the 17th and 18th century in Svalbard and its surrounding seas, which could potentially have had some effect (although unlikely), depending on the used fuel for boiling the whale blubber to oil. Thus, we haven't found a definite explanation for the high contribution of fossil fuel sources to the EC in the ice core in the 1700s and early 1800s, but we can speculate on partial explanations.

3.4. Source Areas Based on Airmass Transport Statistics

General transport patterns of pollutants to the Arctic were more or less established 40 years ago (e.g., Rahn & McCaffrey, 1980) together with the Arctic Haze concept. The Eurasian sector has since been regarded as the main contributor of pollutants to the Arctic. This was confirmed by more detailed later studies of key pollutants (e.g., Hirdman et al., 2010). However, Backman et al. (2021) recently highlighted transport of BC from Asia to the Arctic as being a particularly efficient pathway for pollutants from that region.

Here, we investigate whether different emission source regions could be responsible for different EC deposition observed at the Holtedahlfonna glacier. Because of the long averaging times represented by the ice core samples, single trajectories cannot be assigned to observations. Instead, transport probability maps were compared for relatively low and relatively high EC samples, respectively. The average and the lower and upper quartiles were calculated based on the different EC deposition amounts recorded at Holtedahlfonna between 1948 and 2004. Based on these, the relative difference from the mean in transport probability were calculated for the low and high cases in relation to the average footprint. The resulting geographical distributions are presented in Figure 7. The two cases clearly exhibit organized patterns in different parts of the northern hemisphere. In case of high observed EC deposition at Holtedahlfonna, there is a positive bias in airmasses arriving to the glacier from about the Ural Mountains to the east to about Alaska via Siberia and East Asia (Figure 7a). In cases of low observed EC deposition at the glacier, the sector with positive bias also begins around the Ural Mountains but extend west to about the Atlantic Ocean (Figure 7b). Furthermore, inspection of meteorological parameters (Figure S5 in Supporting Information S1) suggests that low recorded EC values in the ice core are associated with high precipitation and low-level atmospheric transport of EC which indicates strong removal processes of EC from the atmosphere over the Atlantic before arriving at the glacier. The high recorded EC values, on the other hand, are associated with high level transport above the cloud layers, on average low relative humidity, and little precipitation on the route to Svalbard, by subsiding airmasses from aloft originating from East Asia and Siberia. East Asia is a known strong anthropogenic BC emitter (Figure 7d), while also high BC emissions occur over East Siberia from natural wildfires indicated in Figure 7c. Notably, high recorded EC values in the ice core are accompanied by emphasized atmospheric transport from the north-western Russian flaring region (Figures 7a and 7d), while low EC values are recorded in time intervals when airmasses originated remarkably less from this area (Figures 7b and 7d).

Figure 6. Fraction of non-fossil fuel combustion-derived elemental carbon (EC) based on ^{14}C analyses and modeled from organic component results, and comparison of ^{14}C-based contribution of non-fossil-fuel-derived EC in the ice core to biomass-combustion-derived soot-BC in a north-western Russian lake sediment record. (a) The fraction of non-fossil fuel combustion-derived EC is presented in red bars for the time periods covered by the ^{14}C analyses. The same is presented for the modeled results based on organic compound analyses, where the thick blue lines represent the time periods covered by the respective samples. (The dashed lines do not indicate analytical values but connect data points and are intended to follow the respective trend.) (b) Same data as in (a) synthesized over 5 time periods (1715–1860; 1860–1913; 1913–1960; 1960–1992; 1992–2003) to emphasize possible trends. The mean value over the selected time periods is presented as squares, and the range of results is shown by the arrows. The respective number of samples represented by the means is given in numbers next to the arrows. (c) Comparison of the contribution of biomass combustion-derived EC in the Holdahlfonna ice core (red) and soot-BC (SBC) in a northwestern Russian lake sediment core (green, data from Ruppel et al. (2021)) determined by radiocarbon analysis of the respective BC particle fraction.
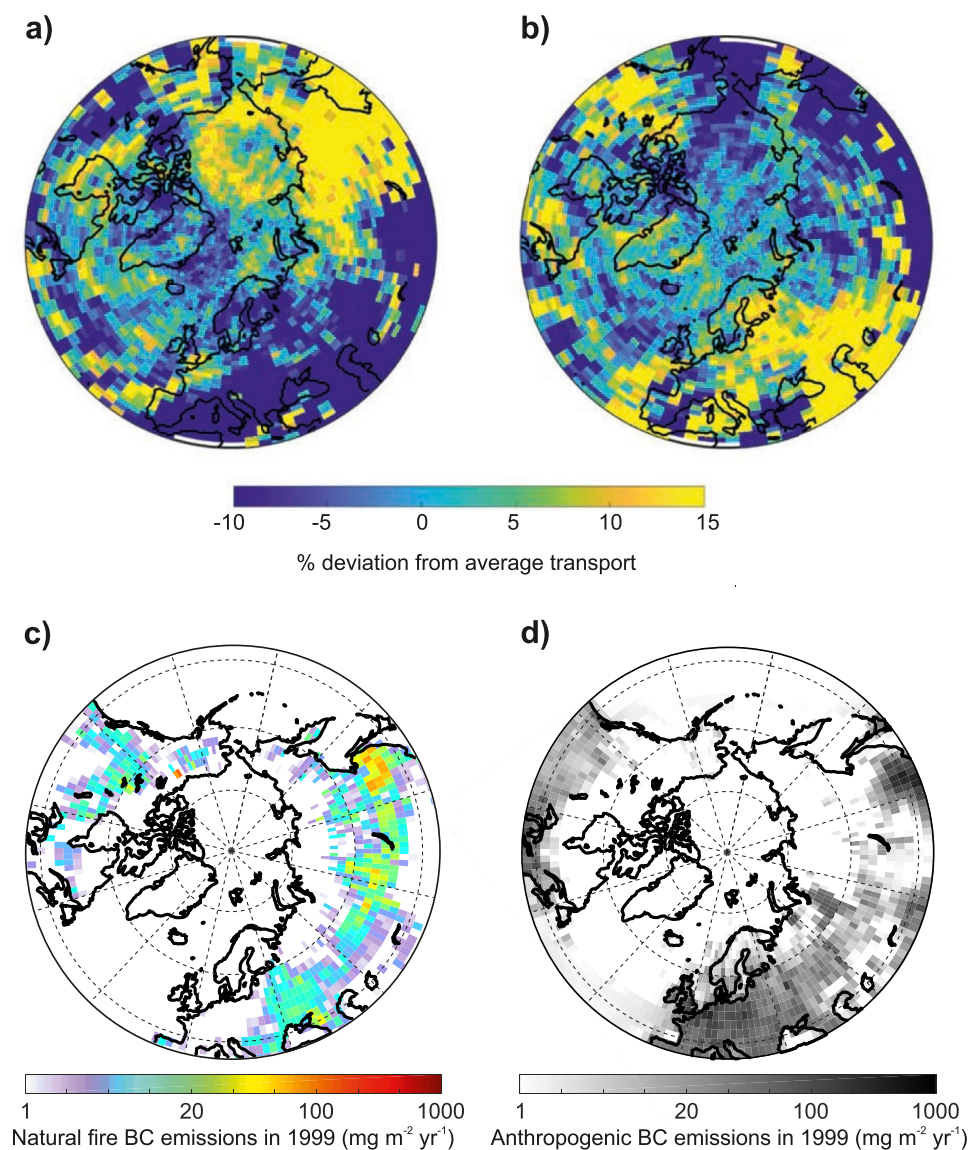
Figure 7. The origin and preferential transport routes for elemental carbon (EC) to the Holtedahlfonna glacier for samples with relatively high and low EC concentrations between 1948 and 2004, and anthropogenic and natural BC emissions in 1999 (mg m^{-2} yr^{-1}). (a) Relative difference in EC source areas for upper quartile (75th percentile) samples, (b) Relative difference in EC source areas for lower quartile (25th percentile) samples, (c) Natural open fire BC emissions in 1999 (data from van Marle et al. (2017)), (d) Anthropogenic BC emissions in 1999 (data from CMIP6, Hoesly et al. (2018)).

Backward calculated trajectories are inherently uncertain especially as the calculated time approaches or exceeds the synoptic time scale. In this comparison additional uncertainties arise from the fact that the meteorological data record starts from a time when the density of observations was much less than today. Nevertheless, our results (Figure 7) consistently suggest subtle changes in atmospheric transport patterns that could be significant for transport and fate of BC in the Arctic. Our results show that not only changes in emissions are responsible for the recorded EC deposition variations at the Holtedahlfonna glacier, but also changes in atmospheric transport patterns. After 1948 atmospheric transport from Asia seems to have become more efficient to the glacier, which is according to the modeling results linked to elevated EC deposition. This suggests that the increasing EC deposition observed in the ice core post-1970 (Figure 2a; Ruppel et al., 2014) is of Asian origin. Thus, the decreasing emissions in Europe (according to emission inventories, e.g., Bond et al., 2007; Hoesly et al., 2018) are not reflected in the ice core EC trend since the glacier has received atmospheric transport increasingly from other more emitting areas in the northern hemisphere which compensated for the decreasing European emissions.

4. Summary and Conclusions

Deciphering EC sources from an ice core record is a complex task. A wide range of different emission sources affect the particles recorded in ice cores at a specific point in time, and these may vary temporally due to changes in the used fuels in different source regions, changes in combustion strength and efficiency, and variations in atmospheric transport to the glacier site. Our analyses of organic compounds, trace elements and radiocarbon together with atmospheric transport modeling present a comprehensive, but at the same time inexhaustive view on sources that have affected the Holtedahlfonna ice core over 300 years. Fossil fuel combustion contributed a large part to the EC deposition at the glacier soon after the beginning of industrialization until WWI, particularly based on the organics and trace element data. A second evident increase in fossil fuel sources occurs toward the end of the record: according to radiocarbon measurements, the peak in fossil fuel use occurred between 1960 and 1990, while the organics and trace element data both (more so the organics) suggest that the contribution of fossil fuels has increased since the 1970s toward the end of the record. Unfortunately, our organic compound and trace element results were not able to help distinguish EC emission sources in more detail than the separation to fossil versus non-fossil fuel sources achieved by the radiocarbon analyses of EC, but the atmospheric modeling results suggested elevated EC deposition recorded at the glacier between 1948 and 2004 to be associated with airmasses arriving from Far East Asia rather than Europe.

Our measurements have shown the applicability of organic compound analyses in the source apportionment of EC in Arctic snow and ice core samples. While this study suffered from incomplete sampling of all organic compounds, that is, the water-soluble part was lost completely, the results show the great potential of these compounds for source apportionment in remote environments. EC source apportionment with help of organic marker compounds may turn out invaluable in the Arctic and other remote regions due to the extremely low sample size required for the analyses (see Section 2.2). The approach presented here to separate the sources of EC based only on the WIOC associated with EC is limited by the lack of specific markers for biomass combustion. Combining this approach with the determination of water-soluble organic components in the filtrate that are specific to biomass combustion, for example, anhydro sugars such as levoglucosan, can certainly improve the discriminatory power of the statistical data analysis.

For comprehensive analysis, snow and ice samples must be properly collected, stored and handled to avoid loss of source markers or contamination of samples, as described in Giorio et al. (2018). This includes collection of filtrates (including WSOC) and filtration residues (including WIOC) and storage of samples in a freezer. Meanwhile, radiocarbon analyses of EC seem to present very robust results on biomass versus fossil fuel sources of EC, even across disciplines and different fractions of BC being analyzed. The caveats of this methodology are, first, the quite large sample amount required, and second, the two-dimensional source separation into only biomass versus fossil fuel sources of EC. Analysis of the stable carbon isotope composition of the EC would enable separating the fossil fuel sources further into coal, liquid fossil fuels and gas flaring facilitating comparison of the analyses with emission sectors commonly used in climate modeling (e.g., Winiger et al., 2017), but these analyses require again a larger sample size which is often challenging to achieve in remote environments. Thus, combining radiocarbon analyses with organic compound analyses presents another possibility to acquire robust and exceptionally comprehensive EC source apportionment from comparably small sample amounts. Here, the radiocarbon measurements are invaluable in quality control of the PMF analyses based on the organic compounds. Trace element, major ion or any other chemical source apportionment analyses may support and work as quality control for EC source apportionment in ice cores.

Data Availability Statement

The numerical measurement analyses data used for EC source apportionment (organic compound and trace element fluxes, and radiocarbon measurements) of the study are available at the Finnish Meteorological Institute repository METIS provided by EUDAT under the CC BY 4.0 open-access license upon publication of the manuscript, https://doi.org/10.23728/fmi-b2share.858bbae80cde4b26bda0a37a56d7db99. Used software for PMF and radiocarbon analyses and HYSPLIT modeling are referenced in the manuscript.

References

Aamaas, B., Bøggild, C. E., Stordal, F., Berntsen, T., Holmén, K., & Ström, J. (2011). Elemental carbon deposition to Svalbard snow from Norwegian settlements and long-range transport. *Tellus*, *63B*(3), 340–351. https://doi.org/10.1111/j.1600-0889.2011.00531.x

AMAP (2015). Black carbon and ozone as Arctic climate forcers. In *Arctic Monitoring and Assessment Programme (AMAP), Oslo* (p. 116).

Andersson, A., Deng, J., Du, K., Yan, C., Zheng, M., Sköld, M., & Gustafsson, Ö. (2015). Regionally-varying combustion sources of the January 2013 severe haze events over eastern China. *Environmental Science and Technology*, *49*(4), 2038–2043. https://doi.org/10.1021/es503855e

Andreae, M. O., & Merlet, P. (2001). Emission of trace gases and aerosols from biomass burning. *Global Biogeochemical Cycles*, *15*(4), 955–966. https://doi.org/10.1029/2000GB001382

Backman, J., Schmeisser, L., & Asmi, E. (2021). Asian emissions explain much of the Arctic Black Carbon events. *Geophysical Research Letters*, *48*(5), e2020GL091913. https://doi.org/10.1029/2020GL091913

Beaudon, E., Gabrielli, P., Sierra-Hernández, M., Wegner, A., & Thompson, L. (2017). Central Tibetan Plateau atmospheric trace metals contamination: A 500-year record from the Puruogangri ice core. *Science of the Total Environment*, *601*, 1349–1363. https://doi.org/10.1016/j.scitotenv.2017.05.195

Beaudon, E., Moore, J. C., Martma, T., Pohjola, V. A., vander Wal, R. S. W., Kohler, J., & Isaksson, E. (2013). Lomonosovfonna and Holtedahlfonna ice cores reveal east-west disparities of Spitsbergen environment since 1700 AD. *Journal of Glaciology*, *59*(218), 1069–1083. https://doi.org/10.3189/2013JoG12J203

Birch, M. E., & Cary, R. A. (1996). Elemental carbon-based method for monitoring occupational exposures, to particulate diesel exhaust. *Aerosol Science and Technology*, *25*(3), 221–241. https://doi.org/10.1080/02786829608965393

Bond, T. C., Bhardwaj, E., Dong, R., Joghani, R., Jung, S., Roden, C., et al. (2007). Historical emissions of black carbon and organic carbon aerosol from energy related combustion, 1850-2000. *Global Biogeochemical Cycles*, *21*(2), GB2018. https://doi.org/10.1029/2006GB002840

Bond, T. C., Doherty, S. J., Fahey, D. W., Forster, P. M., Berntsen, T., DeAngelo, B. J., et al. (2013). Bounding the role of black carbon in the climate system: A scientific assessment. *Journal of Geophysical Research: Atmospheres*, *118*(11), 1–173. https://doi.org/10.1002/jgrd.50171

Brandenberger, S., Mohr, M., Grob, K., & Neukom, H. P. (2005). Contribution of unburned lubricating oil and diesel fuel to particulate emission from passenger cars. *Atmospheric Environment*, *39*(37), 6985–6994. https://doi.org/10.1016/j.atmosenv.2005.07.042

Briggs, N. L., & Long, C. M. (2016). Critical review of black carbon and elemental carbon source apportionment in Europe and the United States. *Atmospheric Environment*, *144*, 409–427. https://doi.org/10.1016/j.atmosenv.2016.09.002

Cavalli, F., Viana, M., Yttri, K. E., Genberg, J., & Putaud, J.-P. (2010). Toward a standardised thermal-optical protocol for measuring atmospheric organic and elemental carbon: The EUSAAR protocol. *Atmospheric Measurement Techniques*, *3*(1), 79–89. https://doi.org/10.5194/amt-3-79-2010

Clarke, A. D., & Noone, K. J. (1985). Soot in the Arctic snowpack: A cause for perturbations in radiative transfer. *Atmospheric Environment*, *19*(12), 2045–2053. https://doi.org/10.1016/0004-6981(85)90113-1

Divine, D., Isaksson, E., Martma, T., Meijer, H. A. J., Moore, J., Pohjola, V., et al. (2011). Thousand years of winter surface air temperature variations in Svalbard and northern Norway reconstructed from ice core data. *Polar Research*, *30*(1), 7379. https://doi.org/10.3402/polar.v30i0.7379

Doherty, S. J., Warren, S. G., Grenfell, T. C., Clarke, A. D., & Brandt, R. E. (2010). Light-absorbing impurities in Arctic snow. *Atmospheric Chemistry and Physics*, *10*(23), 11647–11680. https://doi.org/10.5194/acp-10-11647-2010

Eckhardt, S., Pisso, I., Evangeliou, N., Zwaaftink, C. G., Plach, A., McConnell, J. R., et al. (2023). Revised historical Northern Hemisphere black carbon emissions based on inverse modeling of ice core records. *Nature Communications*, *14*(1), 271. https://doi.org/10.1038/s41467-022-35660-0

Eckhardt, S., Quennehen, B., Olivié, D. J. L., Berntsen, T. K., Cherian, R., Christensen, J. H., et al. (2015). Current model capabilities for simulating black carbon and sulfate concentrations in the Arctic atmosphere: A multi-model evaluation using a comprehensive measurement data set. *Atmospheric Chemistry and Physics*, *15*(16), 9413–9433. https://doi.org/10.5194/acp-15-9413-2015

Evangeliou, N., Shevchenko, V. P., Yttri, K. E., Eckhardt, S., Sollum, E., Pokrovsky, O. S., et al. (2018). Origin of elemental carbon in snow from western Siberia and northwestern European Russia during winter–spring 2014, 2015 and 2016. *Atmospheric Chemistry and Physics*, *18*(2), 963–977. https://doi.org/10.5194/acp-18-963-2018

Forsström, S., Isaksson, E., Skeie, R. B., Ström, J., Pedersen, C. A., Hudson, S. R., et al. (2013). Elemental carbon measurements in European Arctic snow packs. *Journal of Geophysical Research: Atmospheres*, *118*(24), 13614–13627. https://doi.org/10.1002/2013JD019886

Galvão, E. S., de Cassia Feroni, R., & D'Azeredo Orlando, M. T. (2021). A review of the main strategies used in the interpretation of similar chemical profiles yielded by receptor models in the source apportionment of particulate matter. *Chemosphere*, *269*, 128746. https://doi.org/10.1016/j.chemosphere.2020.128746

Giorio, C., Kehrwald, N., Barbante, C., Kalberer, M., King, T. E. R., Wolff, E. W., & Zennaro, P. (2018). Prospects for reconstructing paleoenvironmental conditions from organic compounds in polar snow and ice. *Quaternary Science Reviews*, *183*, 1–22. https://doi.org/10.1016/j.quascirev.2018.01.007

Grieman, M. M., Aydin, M., McConnell, J. R., & Saltzman, E. S. (2018). Burning-derived vanillic acid in an Arctic ice core from Tunu, northeastern Greenland. *Climate of the Past*, *14*(11), 1625–1637. https://doi.org/10.5194/cp-14-1625-2018

Gustafsson, Ö., Kruså, M., Zencak, Z., Sheesley, R. J., Granat, L., Engström, E., et al. (2009). Brown clouds over South Asia: Biomass or fossil fuel combustion? *Science*, *323*(5913), 495–498. https://doi.org/10.1126/science.1164857

Hegg, D. A., Warren, S. G., Grenfell, T. C., Doherty, S. J., & Clarke, A. D. (2010). Sources of light-absorbing aerosol in arctic snow and their seasonal variation. *Atmospheric Chemistry and Physics*, *10*(22), 10923–10938. https://doi.org/10.5194/acp-10-10923-2010

Hirdman, D., Sodemann, H., Eckhardt, S., Burkhart, J. F., Jefferson, A., Mefford, T., et al. (2010). Source identification of short-lived air pollutants in the Arctic using statistical analysis of measurement data and particle dispersion model output. *Atmospheric Chemistry and Physics*, *10*(2), 669–693. https://doi.org/10.5194/acp-10-669-2010

Hoesly, R. M., Smith, S. J., Feng, L., Klimont, Z., Janssens-Maenhout, G., Pitkanen, T., et al. (2018). Historical (1750−2014) anthropogenic emissions of reactive gases and aerosols from the Community Emissions Data System (CEDS). *Geoscientific Model Development*, *11*(1), 369–408. https://doi.org/10.5194/gmd-11-369-2018

Jickells, T. D., Kelly, S. D., Baker, A. R., Biswas, K. F., Dennis, P. F., Spokes, L. J., et al. (2003). Isotopic evidence for a marine ammonia source. *Geophysical Research Letters*, *30*(7), 1374. https://doi.org/10.1029/2002GL016728

Kaspari, S., Mayewski, P., Handley, M., Osterberg, E., Kang, S., Sneed, S., et al. (2009). Recent increases in atmospheric concentrations of Bi, U, Cs, S and Ca from a 350-year Mount Everest ice core record. *Journal of Geophysical Research*, *114*(D4), D04302. https://doi.org/10.1029/2008JD011088

Keegan, K. M., Albert, M. R., McConnell, J. R., & Baker, I. (2014). Climate change and forest fires synergistically drive widespread melt events of the Greenland Ice Sheet. *Proceedings of the National Academy of Sciences USA*, *111*(22), 7964–7967. https://doi.org/10.1073/pnas.1405397111

Koch, D., Bauer, S., Del Genio, A., Faluvegi, G., McConnell, J. R., Menon, S., et al. (2011). Coupled aerosol-chemistry-climate twentieth century transient model investigation: Trends in short-lived species and climate responses. *Journal of Climate*, *24*(11), 2693–2714. https://doi.org/10.1175/2011JCLI3582.1

Lane, D. J., Sippula, O., Koponen, H., Heimonen, M., Peräniemi, S., Lähde, A., et al. (2020). Volatilisation of major, minor, and trace elements during thermal processing of fly ashes from waste- and wood-fired power plants in oxidising and reducing gas atmospheres. *Waste Management*, *102*, 698–709. https://doi.org/10.1016/j.wasman.2019.11.025

Legrand, M., McConnell, J., Fischer, H., Wolff, E. W., Preunkert, S., Arienzo, M., et al. (2016). Boreal fire records in northern hemisphere ice cores: A review. *Climate of the Past*, *12*(10), 2033–2059. https://doi.org/10.5194/cp-12-2033-2016

Legrand, M., Weller, R., Preunkert, S., & Jourdain, B. (2021). Ammonium in Antarctic aerosol: Marine biological activity versus long-range transport of biomass burning. *Geophysical Research Letters*, *48*(11), e2021GL092826. https://doi.org/10.1029/2021GL092826

Liss, P. S., & Galloway, J. N. (1993). Air-sea exchange of sulphur and nitrogen and their interaction in the marine atmosphere. In *Interactions of C, N, P and S biogeochemical cycles and global change* (pp. 259–281). Springer Berlin Heidelberg.

Macdonald, K. M., Sharma, S., Toom, D., Chivulescu, A., Platt, A., Elsasser, M., et al. (2018). Temporally delineated sources of major chemical species in high Arctic snow. *Atmospheric Chemistry and Physics*, *18*(5), 3485–3503. https://doi.org/10.5194/acp-18-3485-2018

Mäkilä, M., Säävuori, H., Kuznetsov, O., & Grundström, A. (2013). Age and dynamics of peatlands in Finland. *Geological Survey of Finland, Report of Peat Investigation*,(Vol. 443, p. 41). in Finnish, abstract in English.

McConnell, J. R. (2010). New Directions: Historical black carbon and other ice core aerosol records in the Arctic for GCM evaluation. *Atmospheric Environment*, *44*(21–22), 2665–2666. https://doi.org/10.1016/j.atmosenv.2010.04.004

McConnell, J. R., & Edwards, R. (2008). Coal burning leaves toxic heavy metal legacy in the Arctic. *Proceedings of the National Academy of Sciences USA*, *105*(34), 12140–12144. https://doi.org/10.1073/pnas.0803564105

McConnell, J. R., Edwards, R., Kok, G. L., Flanner, M. G., Zender, C. S., Saltzman, E. S., et al. (2007). 20th century industrial black carbon emissions altered arctic climate forcing. *Science*, *317*(5843), 1381–1384. https://doi.org/10.1126/science.1144856

Miyake, T., Nakazawa, F., Sakugawa, H., Takeuchi, N., Fujita, K., Ohta, K., & Nakawo, M. (2006). Concentrations and source variations of n-alkanes in a 21m ice core and snow samples at Belukha glacier, Russian Altai mountains. *Annals of Glaciology*, *43*, 142–147. https://doi.org/10.3189/172756406781812159

Mori, T., Kondo, Y., Ohata, S., Zhao, Y., Sinha, P. R., Oshima, N., et al. (2020). Seasonal variation of wet deposition of black carbon in Arctic Alaska. *Journal of Geophysical Research: Atmospheres*, *125*(16), e2019JD032240. https://doi.org/10.1029/2019JD032240

Moschos, V., Dzepina, K., Bhattu, D., Lamkaddam, H., Casotto, R., Dällenbach, K., et al. (2022a). Equal abundance of summertime natural and wintertime anthropogenic Arctic organic aerosols. *Nature Geoscience*, *15*(3), 196–202. https://doi.org/10.1038/s41561-021-00891-1

Moschos, V., Schmale, J., Aas, W., Becagli, S., Calzolai, G., Eleftheriadis, K., et al. (2022b). Elucidating the present-day chemical composition, seasonality and source regions of climate-relevant aerosols across the Arctic land surface. *Environmental Research Letters*, *17*(3), 034032. https://doi.org/10.1088/1748-9326/ac444b

Orasche, J., Schnelle-Kreis, J., Abbaszade, G., & Zimmermann, R. (2011). Technical Note: In-situ derivatization thermal desorption GC-TOFMS for direct analysis of particle-bound non-polar and polar organic species. *Atmospheric Chemistry and Physics*, *11*(17), 8977–8993. https://doi.org/10.5194/acp-11-8977-2011

Orasche, J., Seidel, T., Hartmann, H., Schnelle-Kreis, J., Chow, J. V., Ruppert, H., & Zimmermann, R. (2012). Comparison of emissions from wood combustion. Part 1: Emission factors and characteristics from different small-scale residential heating appliances considering particulate matter and polycyclic aromatic hydrocarbon (PAH)-Related toxicological potential of particle-bound organic species. *Energy & Fuels*, *26*(11), 6695–6704. https://doi.org/10.1021/ef301295k

Oros, D. R., & Simoneit, B. R. T. (1999). Identification of molecular tracers in organic aerosols from temperate climate vegetation subjected to biomass burning. *Aerosol Science and Technology*, *31*(6), 433–445. https://doi.org/10.1080/027868299303986

Oros, D. R., & Simoneit, B. R. T. (2000). Identification and emission rates of molecular tracers in coal smoke particulate matter. *Fuel*, *79*(5), 515–536. https://doi.org/10.1016/s0016-2361(99)00153-2

Osmont, D., Wendl, I. A., Schmidely, L., Sigl, M., Vega, C. P., Isaksson, E., & Schwikowski, M. (2018). An 800-year high-resolution black carbon ice core record from Lomonosovfonna, Svalbard. *Atmospheric Chemistry and Physics*, *18*(17), 12777–12795. https://doi.org/10.5194/acp-18-12777-2018

Paatero, P., & Tapper, U. (1994). Positive matrix factorization: A non-negative factor model with optimal utilization of error estimates of data values. *Environmetrics*, *5*(2), 111–126. https://doi.org/10.1002/env.3170050203

Pacyna, J., & Pacyna, E. (2001). An assessment of global and regional emissions of tracemetals to the atmosphere from anthropogenic sources worldwide. *Environmental Reviews*, *9*(4), 269–298. https://doi.org/10.1139/a01-012

Rahn, K. A., & McCaffrey, R. J. (1980). On the origin and transport of the winter Arctic aerosol. *Annals of the New York Academy of Sciences*, *338*(1), 486–503. https://doi.org/10.1111/j.1749-6632.1980.tb17142.x

Ramanathan, V., & Carmichael, G. (2008). Global and regional climate changes due to black carbon. *Nature Geoscience*, *1*(4), 221–227. https://doi.org/10.1038/ngeo156

Rauber, M., & Salazar, G. (2022). martin-rauber/compycalc. v1.3.0. *Zenodo*. https://doi.org/10.5281/zenodo.7368424

Rauber, M., Salazar, G., Yttri, K. E., & Szidat, S. (2022). An optimised OC/EC fraction separation method for radiocarbon source apportionment applied to low-loaded arctic aerosol filters. EGUsphere. [preprint] https://doi.org/10.5194/egusphere-2022-625

Reff, A., Eberly, S. I., & Bhave, P. V. (2007). Receptor modeling of ambient particulate matter data using positive matrix factorization: Review of existing methods. *Journal of the Air and Waste Management Association*, *57*(2), 146–154. https://doi.org/10.1080/10473289.2007.10465319

Reimer, P. J., Brown, T. A., & Reimer, R. W. (2004). Discussion: Reporting and calibration of post-bomb ¹⁴C data. *Radiocarbon*, *46*(3), 1299–1304. https://doi.org/10.1017/S0033822200033154

Rodríguez, B. T., Huang, L., Santos, G. M., Zhang, W., Vetro, V., Xu, X., et al. (2020). Seasonal cycle of isotope-based source apportionment of elemental carbon in airborne particulate matter and snow at Alert, Canada. *Journal of Geophysical Research: Atmospheres*, *125*(23), e2020JD033125. https://doi.org/10.1029/2020JD033125

Rogge, W. F., Hildemann, L. M., Mazurek, M. A., Cass, G. R., & Simoneit, B. R. T. (1993). Sources of fine organic aerosol. 2. Noncatalyst and catalyst-equipped automobiles and heavy-duty diesel trucks. *Environmental Science and Technology*, *27*(4), 636–651. https://doi.org/10.1021/es00041a007

Rogge, W. F., Hildemann, L. M., Mazurek, M. A., Cass, G. R., & Simoneit, B. R. T. (1997). Sources of fine organic aerosol. 8. Boilers burning No. 2 distillate fuel oil. *Environmental Science and Technology*, *31*(10), 2731–2737. https://doi.org/10.1021/es9609563

Ruggirello, R. M., Hermanson, M. H., Isaksson, E., Teixeira, C., Forsström, S., Muir, D. C. G., et al. (2010). Current-use and legacy pesticide deposition to ice caps on Svalbard, Norway. *Journal of Geophysical Research*, *115*(D18), D18308. https://doi.org/10.1029/2010JD014005

Ruppel, M., Väliranta, M., Virtanen, T., & Korhola, A. (2013). Postglacial spatiotemporal peatland initiation and lateral expansion dynamics in North America and northern Europe. *The Holocene*, *23*(11), 1596–1606. https://doi.org/10.1177/0959683613499053

Ruppel, M. M., Eckhardt, S., Pesonen, A., Mizohata, K., Oinonen, M. J., Stohl, A., et al. (2021). Observed and modeled black carbon deposition and sources in the western Russian arctic 1800-2014. *Environmental Science and Technology*, *55*(8), 4368–4377. https://doi.org/10.1021/acs.est.0c07656

Ruppel, M. M., Gustafsson, Ö., Rose, N. L., Pesonen, A., Yang, H., Weckström, J., et al. (2015). Spatial and temporal patterns in black carbon deposition to dated Fennoscandian Arctic lake sediments from 1830 to 2010. *Environmental Science and Technology*, *49*(24), 13954–13963. https://doi.org/10.1021/acs.est.5b01779

Ruppel, M. M., Isaksson, E., Ström, J., Beaudon, E., Svensson, J., Pedersen, C. A., & Korhola, A. (2014). Increase in elemental carbon values between 1970 and 2004 observed in a 300-year ice core from Holtedahlfonna (Svalbard). *Atmospheric Chemistry and Physics*, *14*(20), 11447–11460. https://doi.org/10.5194/acp-14-11447-2014

Ruppel, M. M., Soares, J., Gallet, J.-C., Isaksson, E., Martma, T., Svensson, J., et al. (2017). Do contemporary (1980–2015) emissions determine the elemental carbon deposition trend at Holtedahlfonna glacier, Svalbard? *Atmospheric Chemistry and Physics*, *17*(20), 12779–12795. https://doi.org/10.5194/acp-17-12779-2017

Sakurai, H., Tobias, H. J., Park, K., Zarling, D., Docherty, K. S., Kittelson, D. B., et al. (2003). On-line measurements of diesel nanoparticle composition and volatility. *Atmospheric Environment*, *37*(9–10), 1199–1210. https://doi.org/10.1016/S1352-2310(02)01017-8

Sand, M., Berntsen, T. K., Seland, Ø., & Kristjánsson, J. E. (2013). Arctic surface temperature change to emissions of black carbon within Arctic or midlatitudes. *Journal of Geophysical Research: Atmospheres*, *118*(14), 1–11. https://doi.org/10.1002/jgrd.50613

Sand, M., Berntsen, T. K., von Salzen, K., Flanner, M. G., Langner, J., & Victor, D. G. (2016). Response of Arctic temperature to changes in emissions of short-lived climate forcers. *Nature Climate Change*, *6*(3), 286–289. https://doi.org/10.1038/nclimate2880

Sankelo, P., Kawamura, K., Seki, O., Shibata, H., & Bendle, J. (2013). n-Alkanes in fresh snow in Hokkaido, Japan: Implications for ice core studies. *Arctic Antarctic and Alpine Research*, *45*(1), 119–131. https://doi.org/10.1657/1938-4246-45.1.119. http://www.jstor.org/stable/23359389

Schauer, J. J., Kleeman, M. J., Cass, G. R., & Simoneit, B. R. T. (1999). Measurement of emissions from air pollution sources. 1. C1 through C29 organic compounds from meat charbroiling. *Environmental Science and Technology*, *33*(10), 1566–1577. https://doi.org/10.1021/es980076j

Schnelle-Kreis, J., Sklorz, M., Orasche, J., Stoelzel, M., Peters, A., & Zimmermann, R. (2007). Semi volatile organic compounds in ambient $PM_{2.5}$. Seasonal trends and daily resolved source contributions. *Environmental Science and Technology*, *41*(11), 3821–3828. https://doi.org/10.1021/es060666e

Schuler, T. V., Kohler, J., Elagina, N., Hagen, J. O. M., Hodson, A. J., Jania, J. A., et al. (2020). Reconciling Svalbard glacier mass balance. *Frontiers in Earth Science*, *8*, 156. https://doi.org/10.3389/feart.2020.00156

Sharma, S., Ishizawa, M., Chan, D., Lavoué, D., Andrews, E., Eleftheriadis, K., & Maksyutov, S. (2013). 16-year simulation of arctic black carbon: Transport, source contribution, and sensitivity analysis on deposition. *Journal of Geophysical Research: Atmospheres*, *118*(2), 943–964. https://doi.org/10.1029/2012JD017774

Sierra-Hernández, M. R., Beaudon, E., Porter, S. E., Mosley-Thompson, E., & Thompson, L. G. (2022). Increased fire activity in Alaska since the 1980s: Evidence from an ice core-derived black carbon record. *Journal of Geophysical Research: Atmospheres*, *127*(2), e2021JD035668. https://doi.org/10.1029/2021JD035668

Sierra-Hernández, M. R., Gabrielli, P., Beaudon, E., Wegner, A., & Thompson, L. G. (2018). Atmospheric depositions of natural and anthropogenic trace elements on the Guliya ice cap (northwestern Tibetan Plateau) during the last 340 years. *Atmospheric Environment*, *176*, 91–102. https://doi.org/10.1016/j.atmosenv.2017.11.040

Sinha, P. R., Kondo, Y., Goto-Azuma, K., Tsukagawa, Y., Fukuda, K., Koike, M., et al. (2018). Seasonal progression of the deposition of black carbon by snowfall at Ny-Ålesund, Spitsbergen. *Journal of Geophysical Research: Atmospheres*, *123*(2), 997–1016. https://doi.org/10.1002/2017JD028027

Sippula, O., Stengel, B., Sklorz, M., Streibel, T., Rabe, R., Orasche, J., et al. (2014). Particle emissions from a marine engine: Chemical composition and aromatic emission profiles under various operating conditions. *Environmental Science and Technology*, *48*(19), 11721–11729. https://doi.org/10.1021/es502484z

Srivastava, R., & Ravichandran, M. (2021). Spatial and seasonal variations of black carbon over the Arctic in a regional climate model. *Polar Science*, *30*, 100670. https://doi.org/10.1016/j.polar.2021.100670

Stein, A. F., Draxler, R. R., Rolph, G. D., Stunder, B. J. B., Cohen, M. D., & Ngan, F. (2015). NOAA's HYSPLIT atmospheric transport and dispersion modeling system. *Bulletin of the American Meteorological Society*, *96*(12), 2059–2077. https://doi.org/10.1175/BAMS-D-14-00110.1

Szidat, S., Salazar, G. A., Vogel, E., Battaglia, M., Wacker, L., Synal, H.-A., & Türler, A. (2014). ¹⁴C analysis and sample preparation at the new Bern Laboratory for the analysis of radiocarbon with AMS (LARA). *Radiocarbon*, *56*(2), 561–566. https://doi.org/10.2458/56.17457

Tian, H. Z., Zhu, C. Y., Gao, J. J., Cheng, K., Hao, J. M., Wang, K., et al. (2015). Quantitative assessment of atmospheric emissions of toxic heavy metals from anthropogenic sources in China: Historical trend, spatial distribution, uncertainties, and control policies. *Atmospheric Chemistry and Physics*, *15*(17), 10127–10147. https://doi.org/10.5194/acp-15-10127-2015

Uglietti, C., Zapf, A., Jenk, T. M., Sigl, M., Szidat, S., Salazar, G., & Schwikowski, M. (2016). Radiocarbon dating of glacier ice: Overview, optimisation, validation and potential. *The Cryosphere*, *10*(6), 3091–3105. https://doi.org/10.5194/tc-10-3091-2016

United States Environmental Protection Agency (2014). Positive matrix factorization model for environmental data analyses [Software]. Version 5.0.0. Retrieved from https://www.epa.gov/air-research/positive-matrix-factorization-model-environmental-data-analyses

vander Wel, L. G., Streurman, H. J., Isaksson, E., Helsen, M. M., Vande Wal, R. S. W., Martma, T., et al. (2011). Using high resolution tritium profiles to quantify the effects of melt on two Spitsbergen ice cores. *Journal of Glaciology*, *57*(206), 1087–1096. https://doi.org/10.3189/002214311798843368

van Marle, M. J. E., Kloster, S., Magi, B. I., Marlon, J. R., Daniau, A.-L., Field, R. D., et al. (2017). Historic global biomass burning emissions for CMIP6 (BB4CMIP) based on merging satellite observations with proxies and fire models (1750-2015). *Geoscientific Model Development*, *10*(9), 3329–3357. https://doi.org/10.5194/gmd-10-3329-2017

Vega, C. P., Björkman, M. P., Pohjola, V. A., Isaksson, E., Pettersson, R., Martma, T., et al. (2015). Nitrate stable isotopes in snow and ice samples from four Svalbard sites. *Polar Research*, *34*(1), 23246. https://doi.org/10.3402/polar.v34.23246

von Schneidemesser, E., Schauer, J. J., Hagler, G. S. W., & Bergin, M. H. (2009). Concentrations and sources of carbonaceous aerosol in the atmosphere of Summit, Greenland. *Atmospheric Environment*, *43*(27), 4155–4162. https://doi.org/10.1016/j.atmosenv.2009.05.043

Wedepohl, K. (1995). The composition of the continental crust. *Geochimica et Cosmochimica Acta*, *59*(7), 12171232–1232. https://doi.org/10.1016/0016-7037(95)00038-2

Winiger, P., Andersson, A., Eckhardt, S., Stohl, A., Semiletov, I. P., Dudarev, O. V., et al. (2017). Siberian Arctic black carbon sources constrained by model and observation. *Proceedings of the National Science Academy USA*, *114*(7), E1054–E1061. https://doi.org/10.1073/pnas.1613401114

Winiger, P., Andersson, A., Yttri, K. E., Tunved, P., & Gustafsson, O. (2015). Isotope-based source apportionment of EC aerosol particles during winter high-pollution events at the Zeppelin Observatory, Svalbard. *Environmental Science and Technology*, *49*(19), 11959–11966. https://doi.org/10.1021/acs.est.5b02644

Winiger, P., Barrett, T. E., Sheesley, R. J., Huang, L., Sharma, S., Barrie, L. A., et al. (2019). Source apportionment of circum-Arctic atmospheric black carbon from isotopes and modeling. *Science Advances*, *5*(2). eaau8052. https://doi.org/10.1126/sciadv.aau8052

World Energy Council. (2013). *World Energy Resources 2013 Survey* (p. 468). World Energy Council.

Yadav, S., Tandon, A., & Attri, A. K. (2013). Monthly and seasonal variations in aerosol associated n-alkane profiles in relation to meteorological parameters in New Delhi, India. *Aerosol and Air Quality Research*, *13*(1), 287–300. https://doi.org/10.4209/aaqr.2012.01.0004

Zdanowicz, C., Gallet, J.-C., Björkman, M. P., Larose, C., Schuler, T., Luks, B., et al. (2021). Elemental and water-insoluble organic carbon in Svalbard snow: A synthesis of observations during 2007–2018. *Atmospheric Chemistry and Physics*, *21*(4), 3035–3057. https://doi.org/10.5194/acp-21-3035-2021

Zennaro, P., Kehrwald, N., McConnell, J. R., Schüpbach, S., Maselli, O. J., Marlon, J., et al. (2014). Fire in ice: Two millennia of boreal forest fire history from the Greenland NEEM ice core. *Climate of the Past*, *10*(5), 1905–1924. https://doi.org/10.5194/cp-10-1905-2014

Zhang, H., Gallego-Sala, A. V., Amesbury, M. J., Charman, D. J., Piilo, S. R., & Väliranta, M. M. (2018). Inconsistent response of Arctic permafrost peatland carbon accumulation to warm climate phases. *Global Biogeochemical Cycles*, *32*(10), 1605–1620. https://doi.org/10.1029/2018GB005980

Zhang, Y. L., Cerqueira, M., Salazar, G., Zotter, P., Hueglin, C., Zellweger, C., et al. (2015). Wet deposition of fossil and non-fossil derived particulate carbon: Insights from radiocarbon measurement. *Atmospheric Environment*, *115*, 257–262. https://doi.org/10.1016/j.atmosenv.2015.06.005

Zhang, Y. L., Perron, N., Ciobanu, V. G., Zotter, P., Minguillón, M. C., Wacker, L., et al. (2012). On the isolation of OC and EC and the optimal strategy of radiocarbon-based source apportionment of carbonaceous aerosols. *Atmospheric Chemistry and Physics*, *12*(22), 10841–10856. https://doi.org/10.5194/acp-12-10841-2012